

Developments of Flat ∞ Coil for Defect Searching in the Curved Surfaces

Kouki MARUYAMA^{1,*}, Iliana MARINOVA^{2,†} and Yoshifuru SAITO¹

¹ Graduate School of Electrical Engineering Hosei University, 3-7-2 Kajino, Koganei, Tokyo 184-8584, Japan

² Technical University of Sofia 1756, Bulgaria

ABSTRACT

Previously we have succeeded in developing a new ECT sensor called ∞ coil. This new ECT sensor is a relatively high sensibility and has the high liftoff characteristics compared with that of conventional ECT sensor.

However, the ∞ coil confronts to a serious difficulty to apply the curved surface specimens. To overcome this difficulty, this paper has worked out a flat ∞ coil. This flat ∞ coil exhibits a high sensitivity not only to the curved surface but also to the flat surface specimens because of its highly shape flexibility to fit the curved target surface and widely spreader-able exciting coils.

Intensive numerical simulations employing 3D FEM have been carried to show the usefulness of the flat ∞ coil. The experimented results have verified the validity of the numerical simulations. Thus, we have confirmed the versatile capabilities of the flat ∞ coil.

KEYWORDS

Eddy current, Non-destructive Testing, Flat ∞ coil, curved surface

Article history:

Received # Month Year

Accepted # Month Year

ARTICLE INFORMATION

1. Introduction

Modern engineering products such as air plane, automobile electric power plant and so on are essentially composed of metallic materials for forming the shape of product, suspending the mechanical stress and constructing the structural frames.

In particular, the mass transportation vehicles carrying a large number of people and various factories e.g. electric power plant and chemical plant are required the ultimately high safety as well as reliability.

To keep the high safety and high quality of their products, the non-destructive testing to the metallic materials is one of the most important technologies because most of the structure materials are composed of the metallic materials.

Various non-destructive testing methods, such as eddy current testing (ECT), ultrasonic testing (UT), radiographic testing (RT) and acoustic emission (AE) are currently used to the modern airplane, high-speed train and express high bus maintenance. Among these methods, ECT does not need complex electronic circuits and direct contact to the tested specimens.

To remove the noise caused by ferromagnetic materials and a circumferential step deformation on the inside surface, an eddy current probe with an original coil arrangement driven by a multi-frequency had been proposed and provided the successful results.[1]

Also, numerical and experimental analysis of eddy current testing for a Tube with Cracks had been carried with fruitful results. [2,3]

Operating principle of the separately installed sensing coil type ECT is fundamentally based on that the sensing coil catches the magnetic field intensity variation caused by the detour eddy currents flowing around a defect in the target metallic materials.[4-6]

To realize this operating principle, three methodologies may be considered. The first detects the

* Corresponding author, E-mail: kouki.maruyama.8n@stu.hosei.ac.jp

† Present address : c/o Y.saito Lab., Graduate School of Electronics and Electrical Engineering Hosei 3-7-2 Kajino-cho Koganei-shi 184-8584, Japan

variation of entire magnetic fields caused by both exciting and eddy currents. In this case, the sensing coil has to detect only a change of the magnetic fields caused by the detour eddy currents around defects from the entire mixed magnetic fields. The second is that the sensing coil surface is installed in a perpendicular direction to the exciting coil surface. This coil layout suggests that the sensing coil never induce an electromotive force due to the exciting fields because the sensing coils are always directed in a parallel direction to the flow of exciting magnetic fields. Thereby, this type is capable of selectively detecting the magnetic fields caused by the detour eddy currents around a defect. The third one is one of the modifications of the second type, i.e., the sensing coil whose axis is perpendicularly crossing to the flow direction of exciting magnetic fields is installed in the zero exciting magnetic field space between the north and south poles of the two exciting coils. A deterministic difference between the second and third ones is exciting magnetic field intensity in the space where the sensing coil is installed. This difference essentially enhances the capability of catching ability only the magnetic fields caused by the detour eddy currents around a defect.

Our laboratory has succeeded in developing the third type ECT sensor called as “ ∞ coil”. This ∞ coil has the high liftoff characteristics compared with those of another type. [4]

However, the ∞ coil confronts to a serious difficulty to apply the curved surface target specimens. To overcome this difficulty, this paper proposes a flat ∞ coil whose exciting coils have a surprising flexibility to fit the curved surface of the target specimens. As a result, it is revealed that this flat ∞ coil has versatile capability, i.e., the defect searching ability not only the curved target specimens but also flat target specimens.

2. The ∞ coils

2.1. Structure of the ∞ coil

Figure.1 shows a typical conventional ∞ coil which is composed of the two finite length solid solenoid coils and one sensing coil wound around the ferrite bar. According to the shape of the two solenoid coils, we have named this sensor as “ ∞ coil”.

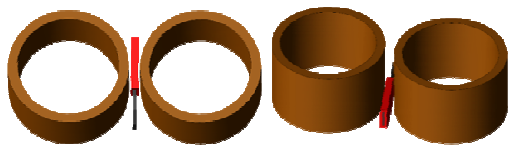


Fig. 1. Structure of the ∞ coil, where circular coils on both side are the exciting coils and the red rectangular boxes are the sensing coils wound around the ferrite bar

Table 1 Various constants used in the 3D simulation

Exciting coil		Sensing coil	
Outer diameter	22.4mm	Outer diameter	1.4×2.4mm
Inner diameter	20mm	Inner diameter	1.0×2.0mm
Length	10mm	Length	6mm
Number of turns	75	Number of turns	100
Input voltage(peak)	1V	Axis core	Mn-Zn/ferrite
Frequency	256kHz		(permeability:3000)

When an alternating current is flowing in series through these two solenoid coils, both coils yield magnetic fields. One becomes a south pole and the other becomes a north pole alternatively. Figure.2 shows an exciting magnetic field intensity distribution computed by the 3D finite elements.

In Fig.2, it is possible to find the zero magnetic field region between the two parallel exciting coils. According to this simulation result, we set a sensing coil wound around the ferrite bar at the bottom of the two exciting coils as shown in Fig.1. Setting the ferrite bar hardly disturbs the exciting magnetic fields because of the weak magnetic field strength location. Thus, the sensor coil wound around a ferrite bar displays an ultimately high sensibility.

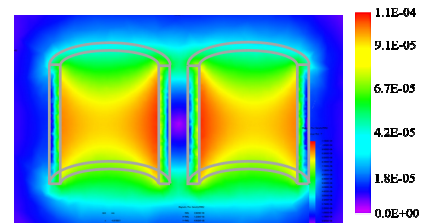


Fig. 2. Magnetic field intensity distribution, where the solid lines denote the parts of exciting coils

2.2. Operating principle of the ∞ coil

The ∞ coil is capable of catching only the magnetic fields caused by the detour eddy currents around a defect. To evaluate the validity of our ∞ coil performance, we have worked out a 3D simulation model as shown in Fig.1. Table 1 lists various constants used in the 3D simulations.

The eddy currents in a plane target specimen (copper plate) located under the two exciting coil surfaces are shown in Fig.3, where the two adjacent exciting coils face to the no-defect, 0 degree, 90 degree and 45 degree line defects as shown in Figs.3(a),3(b),3(c) and 3(d), respectively. Also, Fig.3 shows that the magnetic flux density vector distributions along the axial cross section of the ferrite bar equipped sensor coil are corresponding to that of eddy currents in Figs.3(a),3(b),3(c) and 3(d).

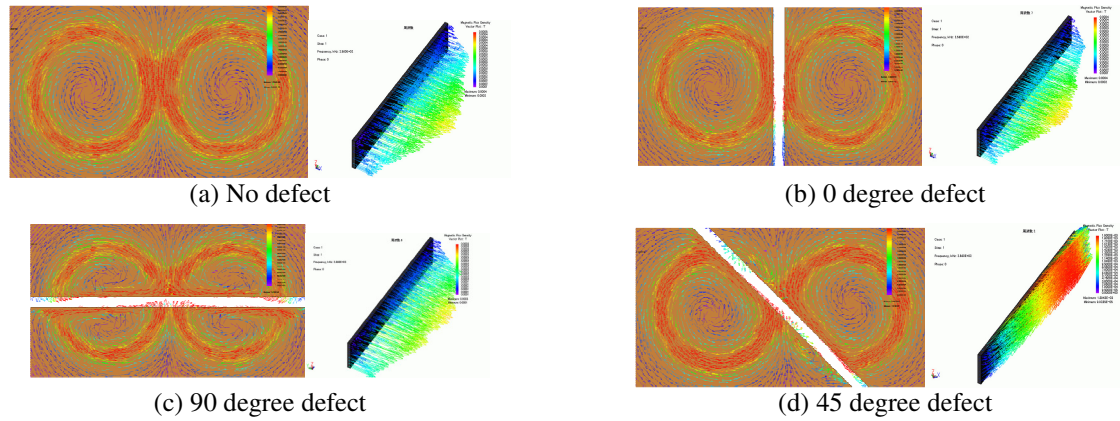


Fig. 3. Eddy currents in a plane copper plate and magnetic flux density vectors in the ferrite bar are shown on the left and right sides in each of the figures (a)-(d), respectively

Color bars in each figures reveals that the uppers and lowers are large and small in values, respectively

Observing the magnetic flux density vector distributions in Fig.3 reveals that the sensing coil wound around the ferrite bar could not induce the electromotive force in the cases of Figs. 3(a), (b) and (c) but induces the electromotive force in the case of Fig.3(d). The induced voltages in the sensor coil under the conditions in Figs. 3 or 3(a)-(d) are shown in Fig.4, whose result reveals that the case (d) yields the highest sensor output voltage.

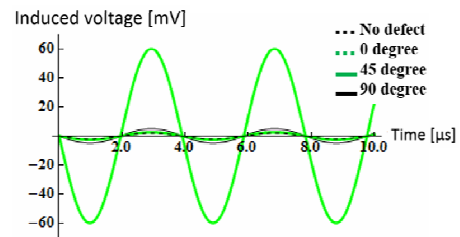


Fig. 4. Induced voltages in the sensing coil

3. The ∞ coil composed of flat and flexible exciting coils

Because of the solid shape of the two solenoid coils, the conventional solid type ∞ coil confronts to a serious difficulty to apply the curved surface target specimens.

To overcome this difficulty, we propose the flat ∞ coil whose exciting coil shape is possible to fit any of the curved surface target specimens. Figure.5 shows a typical shape of the flat ∞ coil.

Figure.6 shows an exciting magnetic field intensity distribution of the flat ∞ coil computed by the 3D finite elements. In Fig.6, it is also possible to find the nearly zero magnetic field strength location between the two parallel flat exciting coils.



Fig. 5. Both of the left and right circular planes are the ∞ coil with flat flexible exciting coils, respectively

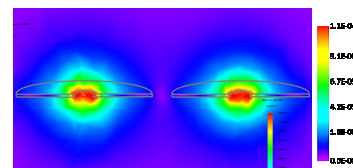


Fig. 6. An example of magnetic field intensity distribution by the flat ∞ coil shown in figure 1

Figures.7(a) and 7(b) show the eddy current distributions caused by the conventional solid and flat ∞ coils, respectively. Observe the results in Fig. 7 suggests that the eddy currents caused by the flat ∞ coil distribute are distributed to wider regions compared with those of the conventional solid ∞ coil. This reveals that the flat ∞ coil has larger searching area.

In addition, the eddy current density of the flat ∞ coil takes higher in magnitude than those of the conventional one because the highest exciting magnetic field strength points caused by the flat ∞ coils exist nearly target piece points as shown in Fig.6. This means that the flat ∞ coil may have ultimately higher sensitivity.

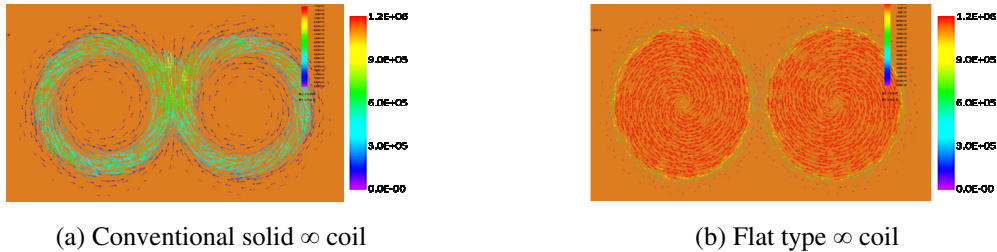


Fig. 7. Eddy current density distributions on the target pieces by the ∞ coils, where the left and right side vectors denote the eddy current density vectors due to the conventional and flat exciting coils, respectively

4. Simulations and Experiments

4.1. Defect searching in a flat surface

We have implemented the sensitivity comparison between conventional solid and flat ∞ coils by simulations as well as experiments. We employed a coppers plate having 1mm thickness and 2mm width defect as a target metal plate specimen. Further, we worked out the two prototypes of the ∞ coils. One is the conventional solid ∞ coil and the other is the flat ∞ coil. Both of these ∞ coils were made with the same conducting coils for the exciting coils having the same number of turns. Table 2 lists various constants of these ∞ coils. Figure.8 shows the pictures of these ∞ coils.

Table 2 Various constants of the tested ∞ coils

(a) Solid type exciting coil		(b) Flat type exciting coil		(c) Sensing coil	
Coil outer diameter	21.0mm	Coil outer diameter	22.0mm	Outer diameter	1.4×2.4mm
Coil Inner diameter	17.0mm	Coil Inner diameter	3.0mm	Inner diameter	1.0×2.0mm
Coil length	8.0mm	Coil length	0.4mm	Length	6mm
Number of turns	20	Number of turns	20	Number of turns	100
Input voltage(peak)	1V	Input voltage(peak)	1V	Axis core	Mn-Zn/ferrite
Frequency	256kHz	Frequency	256kHz		(permeability:3000)

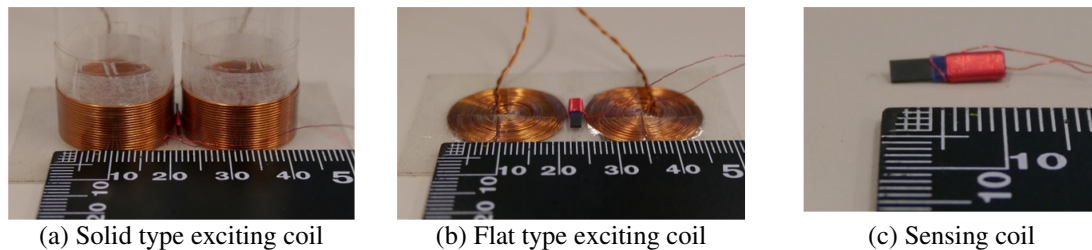


Fig. 8. The pictures of tested ∞ coils, where the left, centre and right denote the conventional, flat ∞ coils and sensing coils wound around a ferrite bar

We measured the induced voltages in the sensing coil when the ∞ coils are located at the No.1, No.2, No.3, No.4 and No.5 points on the target specimen shown in Fig.9. The exciting frequency is 256kHz and exciting voltage is $1V_{Max}$.

We calculated the signal-noise ratio (S/N) from the measured induced voltages by means of equation (1).

$$S/N = \frac{\text{Induced voltages at defect}}{\text{Induced voltages at no defect}} \quad (1)$$

Figures 10 and 11 are the simulation and experimental results for the flat surface searching, respectively. Comparing the induced voltages of flat with those of the conventional solid ∞ coils reveals that the induced voltage of the flat ∞ coil is larger than those of the conventional solid one.

In addition, it is found that the S/N ratios of the flat type ∞ coils take higher in values than those of the conventional solenoid solid one, i.e., experimented S/N ratios of the flat type are 10.89~12.30 and those of the solid type are 7.93~10.79.

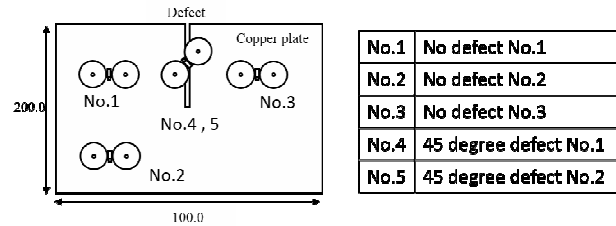


Fig. 9. Schematic diagram of a flat surface searching
 The ∞ coil is located at the center of a perpendicular slit defect. No.4 and No.5 are measured twice at this position to confirm the recoverability of experimented values

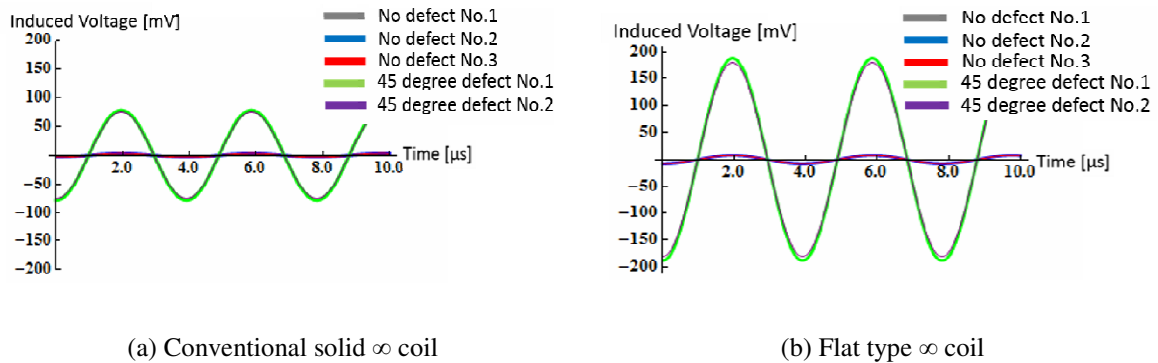


Fig. 10. Simulation results for a flat surface searching

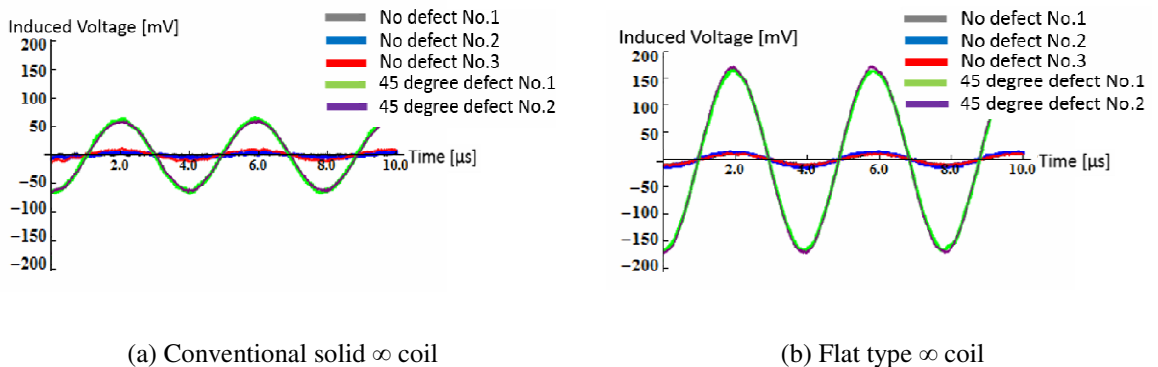


Fig. 11. Experimental results for a flat surface searching

4.2. Defect searching in a curved surface

We employed a seamless pipe having 82mm outer and 54mm inner diameters as a curved surface example. This tested pipe has a 0.3mm width curved line defect as shown in Fig.12.

A 0.3mm width curved line defect shown in Fig.12 is searched by the two distinct sensors. One is

the conventional solid ∞ coil as shown in Fig.8 (a) and the other is the flat ∞ coil as shown in Fig.8 (b).

Figures.13 and 14 show the simulation and experimental results for the curved surface, respectively. Observe the results in Figs.13 and 14 reveals that both of the solid and flat types of ∞ coils obtained by the experimented take the large in valued to that of simulated ones. This may be caused by the idealized simulation and practical measured conditions, i.e. there are many devices and instruments covered as iron case which works as the magnetic flux paths. Also, it is obvious that the flat type ∞ coil has higher sensitivity compared with those of the conventional solid ∞ coil.

The S/N ratios 7.33 and 3.62 by (1) are respectively calculated from the experimented results of the flat and the solid ∞ coils in Fig.14. Because of the fitting property, the S/N ratio 7.33 of the flat ∞ coil is much greater than 3.62 that of solid type ones. This means that the newly developed flat ∞ coil has the versatile capabilities compared with the conventional one.

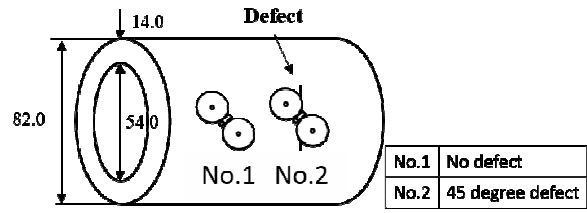
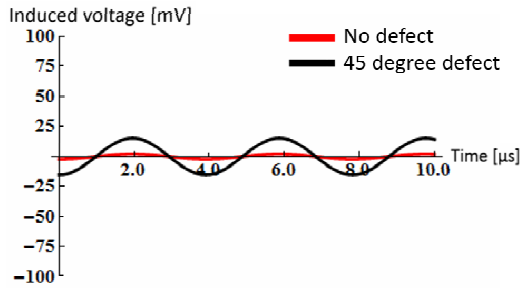
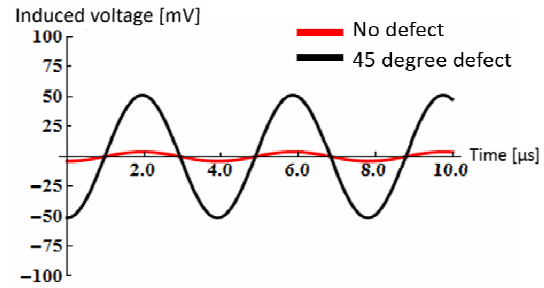


Fig. 12. Schematic diagram of the defect searching of a curved surface

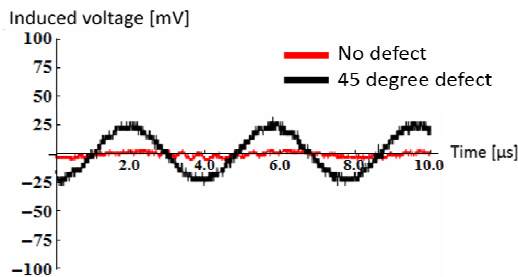


(a) Conventional solid ∞ coil

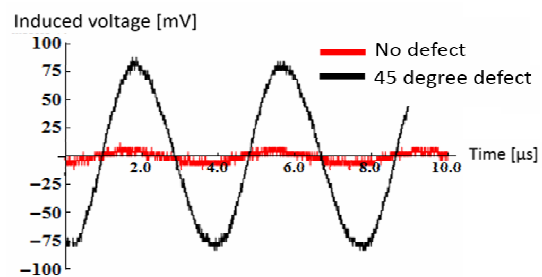


(b) Flat type ∞ coil

Fig. 13. Simulation results for a curved surface searching



(a) Conventional solid ∞ coil



(b) Flat type ∞ coil

Fig. 14. Experimental results for a curved surface searching

5. Conclusion

We have proposed the new ∞ coil which is composed of the flexibly flat exciting coils. Intensive numerical simulations as well as experimental results have elucidated that this newly developed flat ∞ coil has the versatile capabilities compared with the conventional one.

Thus, we have succeeded in developing the new ∞ coil, which has a reasonable capability to detect not only the curved but also flat surface defects in the target.

References

- [1] S.Narishige, A.Nishimizu, M.Koike, Y.Abe, Y.Narumi, T.Tsuge, Improved Detection Performance using a Multi-frequency Method of Eddy Current Testing for Outside Circumferential Cracks near an Expansion of Heat Exchanger Tubes, *Non-Destructive Testing and Condition Monitoring*, Volume 52, Number 6, June 2010, pp. 298-301.
- [2] H.Hashizume, Y.Yamada; K.Miya, S.Toda, K.Morimoto, Y.Araki, K.Satake, N.Shimizu, Numerical and Experimental Analysis of Eddy Current Testing for a Tube with Cracks. *IEEE Trans. Magn.* 1992, 28, 1469-1472.
- [3] M.Morozov, G.Rubinacci, A.Tamburrino, S.Ventre, Numerical Models of Volumetric Insulating Cracks in Eddy-Current Testing with Experimental Validation, *IEEE Trans. Magn.* 2006, 42, 1568-1576.
- [4] Hiroki Kikuchihara, Iliana Marinova, and Yoshifuru Saito, Manabu Ohuch, Hideo Mogi and Yoshiro Oikawa, Optimization of the Eddy Current Testing, *Digest of The 15th Biennial IEEE Conference on Electromagnetic Field Computation WC4-4* pp.495, Oita Japan November 11-14 2012.
- [5] Hiroki Kikuchihara and Yoshifuru Saito, Enhance the Sensibility of the ECT Sensor, *Journal of the Japan Society of Applied Electromagnetics and Mechanics*, Vol.21, No.3 , 2013.
- [6] Kouki Maruyama, Iliana Marinova, and Yoshifuru Saito, Enhance the Sensibility of the Resonance type ECT Sensor, *JAPMED'8* pp. 130-131, 2013.

All Frequency Analysis of Finite Length Solenoid Inductors by Quasi-Analytical Approach

Renya IWANAGA^{1,*}, Iliana MARINOVA², and Yoshifuru SAITO^{1†}

¹ Graduate School of Electrical and Electronic Engineering, Hosei University, Tokyo 184-8584, Japan

² Technical University of Sophia, 1756, Bulgaria

ABSTRACT

Higher frequency operation of the finite length solenoid inductors often leads to a resonance phenomenon. In most case, this is parallel resonance caused the stray capacitances between adjacent coils and the coil inductances. Any of the conventional numerical methods, e.g., FDM and FEM, it is difficult to analysis this resonance, since the original formulation to derive their system of equation never takes both the magnetic and electric fields into account simultaneously. To overcome this difficulty, this paper exploits a quasi-analytical approach to the analysis of resonant phenomena in the finite length solenoid coils which are the conventional exciting coils of the eddy current tests. As a result, we have succeeded in reproduce the parallel resonant phenomena, even though further improvement of our approach is required to solve this all wave problem exactly.

KEYWORDS

all wave analysis, quasi-analytical method, finite length solenoid coil, resonance phenomenon

ARTICLE INFORMATION

Article history:

Received # Month Year

Accepted # Month Year

1. Introduction

To compute the electromagnetic fields, several numerical methods have been proposed and commercial based software packages could be available depending on each of the problems. Even though a lots of packages have been available, it is difficult to evaluate the simple resonant phenomenon of finite length solenoid inductors. This means that an independent solution in each of the Laplace, Poisson, diffusion, wave equations could be easily evaluated but a solution of the mixed problems, e.g., a simultaneous solution of the wave and diffusion equations, is difficult. This leads that there is no commercial based software packages to compute a simple frequency characteristic of finite length solenoid inductors.

Takano and et al. tried to evaluate the exact skin effect of the finite length solenoid inductors and elucidated that two kind of skin effects are observed in the finite length solenoid inductors. One is a local skin effect observed in each of the cross-sections of the conductors and the other is a global skin effect to reduce the linkage fluxes as possible as small in entire inductors [1].

Watazawa and et al. tried to evaluate a quasi-analytical solution of the Laplace, Poisson, diffusion, wave mixed problem and elucidated the fundamental difference between the skin and proximate effects [2].

Xin Hu developed a full wave solver. Probably this is the first general purpose solver to the mixed problems [3].

This paper tries to carry out the quasi-analytical solution of the exact spirally wound finite length solenoid inductor which is frequency used as the exciting coils of the eddy current tests. Even though the quasi-analytical solutions are not exactly corresponding to that of experimental ones, it is clarified that the resonant phenomenon is possible to evaluate by means of the quasi-analytical approach proposed in this paper.

* Renya IWANAGA, E-mail: renya.iwanaga.3a@stu.hosei.ac.jp

† Present address : c/o Y.Saito., Graduate School of Electronics and Electrical Engineering Hosei 3-7-2 Kajinotyou Koganei 184-8584, Japan

2. Quasi-Analytical Approach

2.1. Principle

As an example, let us consider the impedance on a finite length solenoid inductor of n -turns shown the Fig.1(a). As shown in Fig.1(b), the finite length solenoid inductor is subdivided into the m^{th} conductors in each of the turns.

One turn of finite length solenoid inductor is one of the circles not connected the start and end points. This circle is subdivided into m^{th} small conductors having circular cross-section



(a) Original finite length solenoid inductor. (b) Modeling of finite length solenoid inductor.

Fig.1 A finite length solenoid inductor and its modeling.

Fig.2 shows the two parallel located subdivisions in the i^{th} small conductors having circular cross-section.

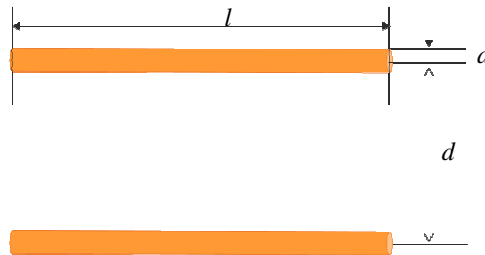


Fig.2 Two parallel located subdivisions in the i^{th} small conductors having circular cross-section.

Since the shape of a subdivided small conductor in Fig. 1(b) or 2 is a simple cylindrical form, it is possible to apply the classical analytical formulae for the inductance, resistance and capacitance calculations. **The analytical solution by means of a Bessel function leads to the skin effect when the current is uniformly distributed. Thereby, this skin effect could be taken into account in each of the small conductors. Namely,** the resistance r , self-inductance L are respectively given by (2)-(4). In Eqs.(1)-(8), σ , μ_0 , l , a , and S are the resistivity, permeability of air, length of a conductor, radius of the subdivided conductor and cross-sectional area, respectively.

$$k = a \sqrt{\frac{\omega \mu \pi}{2 \rho}} \quad (1)$$

(a) If supply angular frequency ω is small, and $k < 1$,

$$L = L_i + L_o = \frac{\mu_0 l}{2} \left(1 - \frac{1}{6} k^4 \right) + \frac{\mu_0}{2 \pi} \left[l \ln \left(\frac{l + \sqrt{a^2 + l^2}}{a} \right) - \sqrt{a^2 + l^2} + a \right] \quad (2-a)$$

$$R = R_D \left(1 + \frac{1}{3} k^4 \right) \quad (3-a)$$

(b) If supply angular frequency ω is large, and $k > 1$,

$$L = L_i + L_o = \left(\frac{\mu_0 l}{2\pi} \right) \left\{ \left(\frac{1}{k} - \left(\frac{1}{64 k^3} \right) \right) \right\} + \frac{\mu_0}{2\pi} \left[l \ln \left(\frac{l + \sqrt{a^2 + l^2}}{a} \right) - \sqrt{a^2 + l^2} + a \right] \quad (2-b)$$

$$R = R_D \left(\frac{1}{4} + k + \frac{1}{64 k^3} \right) \quad (3-b)$$

where R_D is the DC resistance,

$$R_D = \frac{\rho l}{\pi a^2} \quad (4)$$

There is a mutual coupling between the cylindrical conductors in Fig.2 because of the common magnetic fluxes. This mutual coupling is represented in terms of the mutual inductance M_{ij} ($i = 1, 2, 3, \dots, m$, $j = 1, 2, 3, \dots, m$, $i \neq j$). In addition, the mutual inductance through the entire solenoidal coil should be taken into account as one of the magnetic couplings.

$$M_{ij} = \frac{\cos \theta \times \mu_0}{2\pi} \left[\ln \left(\frac{l + \sqrt{l^2 + d_{ij}^2}}{d_{ij}} \right) - \sqrt{1 + \left(\frac{d_{ij}}{l} \right)^2} + \frac{d_{ij}}{l} \right] \quad (7)$$

The displacement current between the cylindrical conductors in Fig.2 is represented in terms of the current through the capacitances C_{ij} ($i = 1, 2, 3, \dots, m$, $j = 1, 2, 3, \dots, m$, $i \neq j$). According to a lots of numerical simulations, it has been found that the capacitance two adjacent conductors in Fig. 2 should be taken into account by (8) where ϵ_r is the relative permittivity.

$$C_{ij} = \frac{\epsilon_r \epsilon_0 S_{ij}}{d_{ij}} \quad (8)$$

The reference point for the capacitance calculation among the small subdivided conductors is assumed at a midpoint in each of the conductors. The other circuit parameters are calculated by the common use of this reference point. In (9), the subscripts i and j refer to the i^{th} and j^{th} cylindrical conductors, respectively. Also, d_{ij} and S_{ij} are the distance and area between the i^{th} and j^{th} cylindrical conductors.

Thus, an entire impedance of finite length solenoid inductor is reduced into the evaluations of the branch currents and the nodal voltages at all of the circuits, e.g., Fig. (3) shows the simplest equivalent circuit representation of the problem.

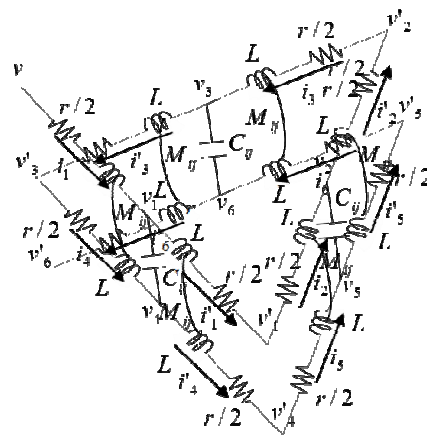


Fig.3 Example of the equivalent circuit, when the inductor has 2 turn, and number of subdivision is 3 in every turn.

2.2. System of equations

Denoting \mathbf{X} and \mathbf{Y} are respectively the state variable vector (10) and input vector (11), a system of equations (9) is written as:

$$\mathbf{Y} = \mathbf{D}\mathbf{X} \quad (9)$$

$$\mathbf{X} = [i_1 \ i_2 \ \dots \ i_{(m \times n)} \ i'_1 \ i'_2 \ \dots \ i'_{(m \times n)} \ v_1 \ v_2 \ \dots \ v_{(m \times n)} \ v'_1 \ v'_2 \ \dots \ v'_{(m \times n-1)}]^T \quad (10)$$

$$\mathbf{Y} = [v_{in} \ 0 \ 0 \ \dots \ 0]^T \quad (11)$$

A state transition matrix \mathbf{D} in (9) is composed of the several sub-matrices as shown in (13).

$$\mathbf{D} = \begin{bmatrix} \mathbf{R} + \mathbf{L} + \mathbf{M} & \mathbf{M} & \mathbf{I}_{D(m \times n)} & -\mathbf{K}_1 \\ \mathbf{M} & \mathbf{R} + \mathbf{L} + \mathbf{M} & -\mathbf{I}_{D(m \times n)} & \mathbf{K}_2 \\ \mathbf{I}_{D(m \times n)} & -\mathbf{I}_{D(m \times n)} & \mathbf{C} & \mathbf{0} \\ \mathbf{K}_1^T & -\mathbf{K}_2^T & \mathbf{0} & \mathbf{0} \end{bmatrix} \quad (12)$$

$$\mathbf{R} = \begin{bmatrix} r & 0 & \dots & 0 \\ 0 & r & & \cdot \\ \cdot & \cdot & \cdot & \cdot \\ \cdot & & r & 0 \\ 0 & \cdot & \cdot & 0 & r \end{bmatrix} \quad \mathbf{M} = \begin{bmatrix} 0 & j\omega M_{12} & \dots & j\omega M_{1j} \\ j\omega M_{21} & 0 & & j\omega M_{2j} \\ \cdot & \cdot & \cdot & \cdot \\ \cdot & \cdot & \cdot & \cdot \\ j\omega M_{i1} & j\omega M_{i2} & \dots & 0 \end{bmatrix}^T$$

$$\mathbf{L} = \begin{bmatrix} j\omega L & 0 & \dots & 0 \\ 0 & j\omega L & & \cdot \\ \cdot & \cdot & \cdot & \cdot \\ \cdot & & j\omega L & 0 \\ 0 & \cdot & \cdot & 0 & j\omega L \end{bmatrix} \quad \mathbf{C} = \begin{bmatrix} -j\omega C_{1j} & 0 & \dots & 0 & j\omega C_{1j} & \dots & 0 \\ 0 & -j\omega C_{2j} & & & & & \cdot \\ \cdot & \cdot & \cdot & \cdot & \cdot & \cdot & \cdot \\ \cdot & \cdot & \cdot & \cdot & \cdot & \cdot & \cdot \\ \cdot & \cdot & \cdot & \cdot & \cdot & \cdot & \cdot \\ \cdot & \cdot & \cdot & \cdot & \cdot & -j\omega C_{(i-1)j} & 0 \\ 0 & \dots & j\omega C_{ij} & 0 & \cdot & 0 & -j\omega C_{ij} \end{bmatrix}$$

$$\mathbf{K}_1 = \begin{bmatrix} 0 & \dots & 0 \\ 1 & \cdot & \cdot \\ 0 & \cdot & \cdot \\ \cdot & \cdot & 0 \\ 0 & \cdot & 0 & 1 \end{bmatrix} \quad \mathbf{K}_2 = \begin{bmatrix} 1 & 0 & \dots & 0 \\ 0 & \cdot & & \cdot \\ \cdot & \cdot & \cdot & 0 \\ \cdot & & & 1 \\ 0 & \cdot & \cdot & 0 \end{bmatrix} \quad (13)$$

where $\mathbf{I}_{D(m \times n)}$ $\mathbf{0}$ are the identity and zero matrices, respectively.

The state transition matrix \mathbf{D} is square matrix so that it is possible to take the inverse matrix \mathbf{D}^{-1} . This leads to the solution vector \mathbf{X} by (14).

$$\mathbf{X} = \mathbf{D}^{-1}\mathbf{Y} \quad (14)$$

By means of (14), the current vector \mathbf{I} and the impedance Z of finite length solenoid inductor could be obtained by (15) and (16), respectively.

$$\mathbf{I} = [i_1 \ i_2 \ \dots \ i_{(m \times n)} \ i'_1 \ i'_2 \ \dots \ i'_{(n \times m)}] \quad (15)$$

$$Z = v_{in} / |i'_{(n \times m)}| \quad (16)$$

3. Example

Let us **calculate** the impedance in finite length solenoid inductor shown in Fig.1(a) when impressing a sinusoidal voltage. Table 1 lists various constants used in the **calculations**.

Table.1 Various constants used in the **calculation** of a finite length solenoid inductor.

Material	Copper
Resistivity	$1.72 \times 10^{-8} [\Omega \cdot \text{m}]$
Dimensions	Diameter:2[cm] × Length:2.2[cm]
Number of turns	20
Coil diameter	0.5[mm]
Number of subdivisions (one turn)	1000(50)
Impressed voltage	1.0[V _{rms}]

Fig.4 shows a comparison between the impedance vs. frequency characteristics calculated by our **quasi-analytical approach** and **experimental one**.

In Fig.4, a parallel resonance could be observed in the frequency characteristics of our model. Comparing the two **frequency characteristics** reveals that their **frequency characteristics** take in a manner even though the values of the impedance as well as resonant frequency are different.

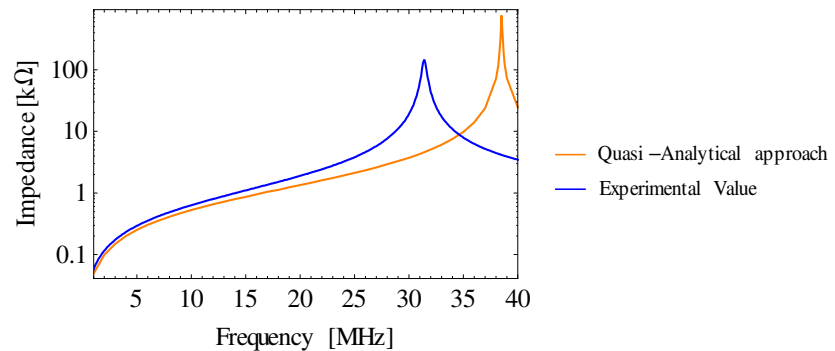
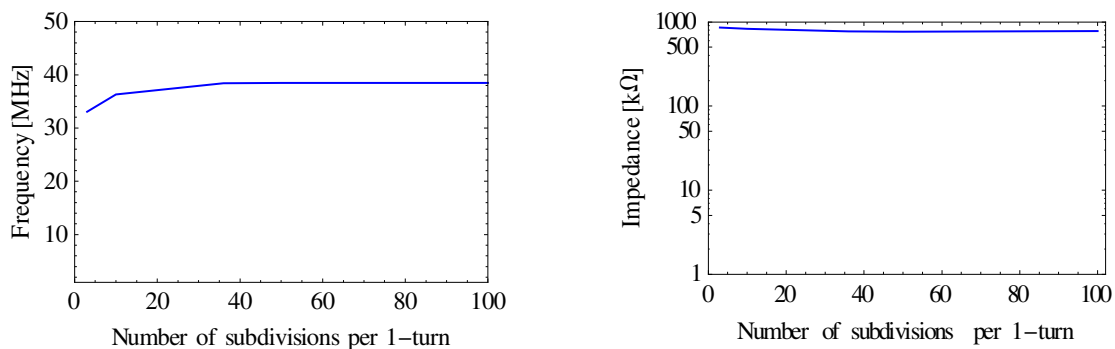


Fig.4 Comparison between the impedances obtained by the quasi-analytical approach and experimented

Fig.5(a) summarizes a relationship between the resonant frequency and the number of subdivisions m . Fig.5(b) summarizes a relationship between the resonant impedance and the number of subdivisions m .



(a) A relationship between the resonant frequency and the number of subdivisions m .

(b) A relationship between the resonant impedance and the number of subdivisions m .

Fig.5 Relationships among the number of the subdivisions m in every turn.



Figs.5(a) and 5(b) show that both of the resonant frequency and impedance at resonant frequency are converged to a constant values when increasing the number of subdivisions.

Thus, it is clarified that a sufficiently large number of subdivisions $m \geq 50$ is essential to calculate the frequency characteristics of the finite length solenoid inductors by the quasi-analytical approach.

4. Conclusion

In this paper, we have proposed the new quasi-analytical approach taking into account accurate shape of inductor and the stray capacitances among conductors.

As a result, it has been clarified that the resonance phenomenon of the finite length solenoid inductors could be reproduced by our quasi-analytical approach **although** further improvement is required **to evaluate the exact results**.

References

- [1] T.Takano, S.Hayano, and Y.Saito, Coil impedance computation having arbitrary geometrical shape, IEEE PESC'98, Vol.2, May 1998.
- [2] Yasuyuki Watazawa, Seiji Hayano and Yoshifuru Saito, Semi-analytical electromagnetic field Computation, Int. J. Appl. Electromagn. Mater. Vol.15,Nos.1-4, pp. 353–357, 2002.
- [3] Xin Hu, Full-wave Analysis of Large Conductor Systems over Substrate, Ph.D Theses MIT, January 2006.

Harmonic Balance Analysis for Magnetic Hysteresis under Static and Dynamic Stresses

Hideaki NEMORI^{1,*}, Iliana MARINOVA², and Yoshifuru SAITO¹

¹ Graduate School of Electrical and Electronics Engineering, Hosei University, Tokyo 184-8584, Japan

² Technical University of Sofia 1756, Bulgaria

ABSTRACT

To evaluate a stress effect to the ferromagnetic properties, this paper proposes a methodology utilizing a frequency response of the domain based magnetization model. A key idea of this approach is based on the following facts that the parameters identification of a domain based magnetization model has been successfully developed by a harmonic balance approach. Since the parameters of the model are extremely sensitive to the various measurement conditions such as temperature, mechanical stress and so on, investigation to the model parameter deflection while controlling a particular measurement condition reveals its controlled parameter effect to the tested ferromagnetic materials. As a result, it is found that the stress effect to a parameter expressing hysteretic property has been clearly deflected its values depending on the externally applied stresses.

KEYWORDS

ferromagnetic material, domain based model, hysteretic property, harmonic balance, Fourier series

ARTICLE INFORMATION

Article history:

Received # Month Year

Accepted # Month Year

1. Introduction

As is well known, ferromagnetic materials exhibit a lot of complex physical properties, such as magnetization, magnetostriction and magneto-thermodynamic properties. Any of these physical properties are nonlinear properties as, detailed relationships among them are still unknown.

Recently we have tried to identify the parameters of magnetization model by a harmonic balance approach [1-3]. As a result, exact magnetization characteristics have been successfully reproduced from the input field intensity H as well as output flux density B measurements even if the deeply saturated situation. Of course, magnetization model had been essentially required so that we had employed a domain based magnetization model.

To keep the ultimate safety, this paper focuses on a stress effect to the parameters of this model, because most of the mechanical frame structures of the industrial products, e.g., car, aircraft, high speed train and so on are always composed of the iron or its composites, i.e., ferromagnetic materials. Particularly, their nonlinear magnetization characteristics are function of externally impressed stresses. This is because some external physical energy is added to their domain structures so that their structures are essentially stimulated to change[4-6].

Even if a not pressured condition, the magnetic nonlinear problems are extensively solved by means of harmonic balanced approach [7-10].

On the other side, we apply the orthogonal property between the odd and even functions of the Fourier series to decide the parameters of the domain based constitutive equations under both no and pressured conditions, i.e., one of the novel applications of the harmonic balanced approach is proposed in this paper.

At first, we introduce the domain based model and describe the physical meanings in each of its parameters. Second, to determine the coefficients of the domain based model, we apply orthogonal

* Corresponding author, Hideaki.NEMORI, E-mail: hideaki.nemori.4p@stu.hosei.ac.jp

† Present address: c/o Y.Saito Lab. Graduate School of Electronics and Electrical Engineering, Hosei University, Tokyo-184-8584, Japan.

properties of the sinusoidal and cosinusoidal functions.

Finally, it is clarified that the most sensitive stress effect factor is a parameter expressing hysteretic property.

2. Domain Based Model

2.1. Domain Based Model and Its Parameters

Previously, we have proposed two types of constitutive models for representing the ferromagnetic properties, i.e., phenomenological and domain based models [1,2]. This paper employs the domain based model [2], and the relationship between the magnetic field $H[A/m]$ and flux density $B[T]$ is represented by the domain based model as

$$H = \frac{1}{\mu} B + \frac{1}{s} \frac{dB}{dt} - \frac{\mu_r}{s} \frac{dH}{dt} \quad (1)$$

where μ , μ_r and s are the permeability measured in the ideal magnetization curve, reversible permeability measured along with the ideal magnetization curve, and hysteresis coefficient, respectively [1-3].

2.2. Harmonic Balance Method

Let us consider an input and output system shown in Fig.1. When the input and output of this system are respectively given by

$$f(t) = \sum_{i=1}^n a_i \sin(i\omega t) + \sum_{i=1}^n b_i \sin(i\omega t) \quad (2)$$

$$g(t) = \sum_{i=1}^n c_i \sin(i\omega t) + \sum_{i=1}^n d_i \sin(i\omega t) \quad (3)$$

We represent this system by a following constitutive equation

$$f(t) = \frac{1}{\mu} g(t) + \frac{1}{s} \frac{dg(t)}{dt} - \frac{\mu_r}{s} \frac{df(t)}{dt} \quad (4)$$

An alternative form of (4) is

$$f(t) = \alpha g(t) + \beta \frac{dg(t)}{dt} - \gamma \frac{df(t)}{dt} \quad (5)$$

To determine the parameter α , β , γ , in (5), multiply the output function $g(t)$ to both sides of (5) and integrate from 0 to T yields.

$$\int_0^T g(t) f(t) dt = \alpha \int_0^T g(t) g(t) dt + \beta \int_0^T g(t) \frac{dg(t)}{dt} dt - \gamma \int_0^T g(t) \frac{df(t)}{dt} dt \quad (6)$$

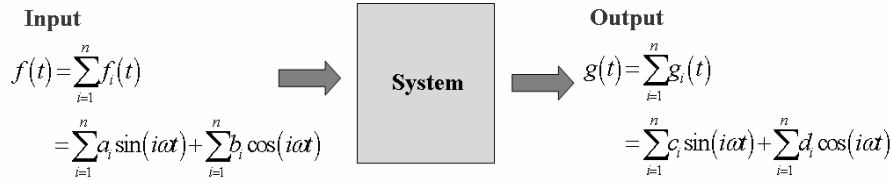


Fig. 1. Simple input and output system.

Similarly multiply the time derivative of output function $dg(t)/dt$ to both sides of (5) and integrate from 0 to T yields

$$\int_0^T \frac{dg(t)}{dt} f(t) dt = \alpha \int_0^T \frac{dg(t)}{dt} g(t) dt + \beta \int_0^T \frac{dg(t)}{dt} \frac{dg(t)}{dt} dt - \gamma \int_0^T \frac{dg(t)}{dt} \frac{df(t)}{dt} dt \quad (7)$$

Further, multiply the input function $f(t)$ to both sides of (5) and integrate from 0 to T yields

$$\int_0^T f(t) f(t) dt = \alpha \int_0^T f(t) g(t) dt + \beta \int_0^T f(t) \frac{dg(t)}{dt} dt - \gamma \int_0^T f(t) \frac{df(t)}{dt} dt \quad (8)$$

Substituting the input (2) and output (3) functions into the equations (6), (7) and (8), it is possible to set up a system of equations for i -th harmonics as

$$\begin{bmatrix} a_i c_i + b_i d_i \\ b_i c_i - a_i d_i \\ a_i^2 + b_i^2 \end{bmatrix} = \begin{bmatrix} c_i^2 + d_i^2 & 0 & -i\omega(a_i d_i - b_i c_i) \\ 0 & i\omega(c_i^2 + d_i^2) & -i\omega(a_i c_i + b_i d_i) \\ a_i c_i + b_i d_i & -i\omega(a_i d_i - b_i c_i) & 0 \end{bmatrix} \cdot \begin{bmatrix} \alpha_i \\ \beta_i \\ \gamma_i \end{bmatrix} \quad (9)$$

Input and output relation for i -th harmonics is given by

$$f_i(t) = \alpha_i g_i(t) + \beta_i \frac{dg_i(t)}{dt} - \gamma_i \frac{df_i(t)}{dt} \quad (10)$$

Let us introduce a phaser notation, i.e., a symbol $\hat{}$ refers to complex quantities, then (10) could be reduced into

$$(1 + j\omega\gamma_i) \hat{f} = (\alpha_i + j\omega\beta_i) \hat{g}, \quad (11)$$

where

$$j = \sqrt{-1} \quad (12)$$

Thus, the output is

$$g(t) = \sum_{i=1}^n \frac{1 + (i\omega\gamma_i)^2}{\alpha_i^2 + (i\omega\beta_i)^2} \sqrt{f_{i,r}^2 + f_{i,l,m}^2} \cos\left(i\alpha t - \tan^{-1} \frac{f_{i,l,m}}{f_{i,r}} + \tan^{-1} i\omega\gamma_i - \tan^{-1} \frac{i\omega\beta_i}{\alpha_i}\right) \quad (13)$$

Entire sum of the output (13) for i -th harmonics gives the output g of (3).

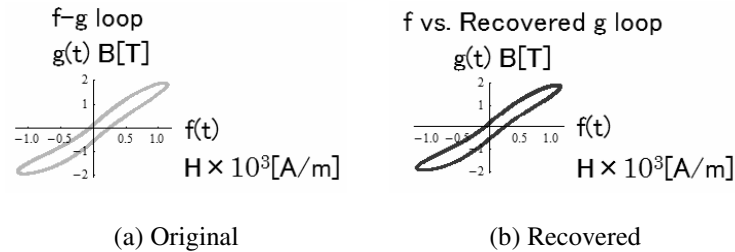


Fig 2. Validity check of the model (4) or (5)

Figure 2 shows one of the examples of the recoverability of our domain based harmonic balance solution. According to the result shown in Fig.2, it is obvious that the nonlinear magnetization characteristics exhibiting the hysteretic properties of ferromagnetic fields could be solved by means of phaser transform method.

3. Experiment

3.1. Experimental Verifications

Figure 3 shows an experimental device and Table 1 lists its various constants. The tested specimens are the silicon steels with the 0.35mm thickness, 30mm width and 100mm length. The tested specimen was put on the upper two head surfaces of U shape ferrite core wound the 300 turns exciting coil. The specimen in Fig.3 is excited by an alternating current having 0.35A peak value through this exciting coil.

Table 1 Specification of the measurement devices

Specimen	U shape ferrite core
Material: silicon steels	Material: ferrite
Length: 100cm	Number of coil turns: 300 turns
Width: 30mm	Diameter of conductor: 0.6mm
Thickness: 0.35mm	
Number of coil turns: 300 turns	
Diameter of conductor: 0.2mm	

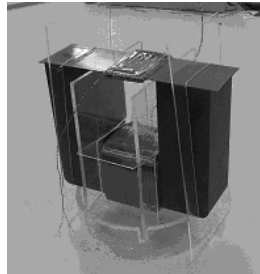


Fig 3. Specimen and U shape ferrite core

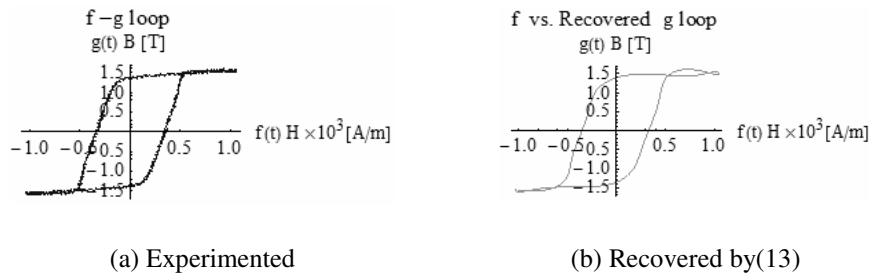


Fig 4. Comparison between the experimental and recovered hysteresis loops

Figure 4 shows a comparison between the experimented and recovered hysteresis loops. Recovered hysteresis loop by (13) is well corresponding to experimental one. A correlation coefficient between the Figs. 4(a) and 4(b) is over 0.99. This means that the hysteretic nonlinear magnetization problems in ferromagnetic fields could be solved by means of the harmonic balance approach.

3.2. Stress Visualization

Figure 5 shows an experimental schematic diagram to visualize the applied stress. A U shape ferrite core wound the exciting coil just same as shown in Fig.3. The specimen wound the search coil is put on the upper two head surfaces of U shape ferrite core. The stress was applied to the specimen by putting on the wood weight to the specimen as shown in Fig 6. The used weight is 900g.

Figure 6 shows the hysteresis loops when applied the 900g stress. Figures 6(a), 6(b) and 6(c)

show the hysteresis loops when impressing low, middle and high voltages, respectively.

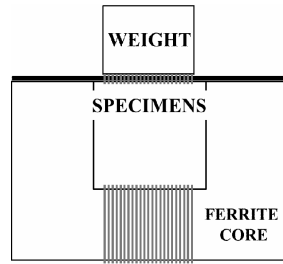


Fig 5. Schematic diagram of the stress impression

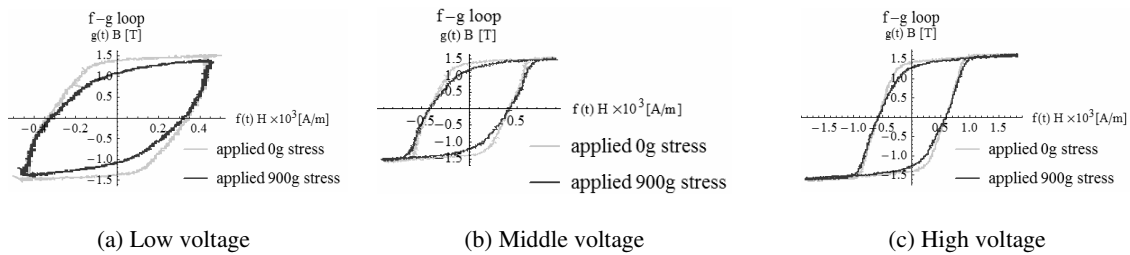


Fig 6. Difference of the hysteresis loops between the no mechanical stress and 900g stress conditions.

Observe the results in Fig. 6 reveals that the hysteresis loops are changing in accordance with the 900g stress impression.

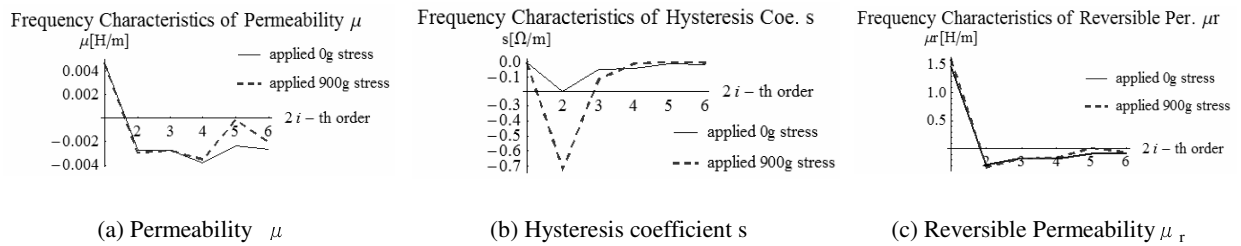


Fig 7. Parameters μ , s , and μ_r values in each of the harmonics when impressing low exciting voltage.

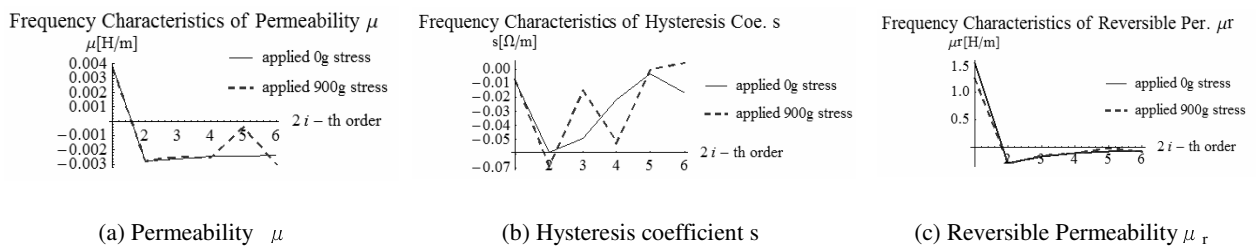


Fig 8. Parameters μ , s , and μ_r values in each of the harmonics when impressing middle exciting voltage.

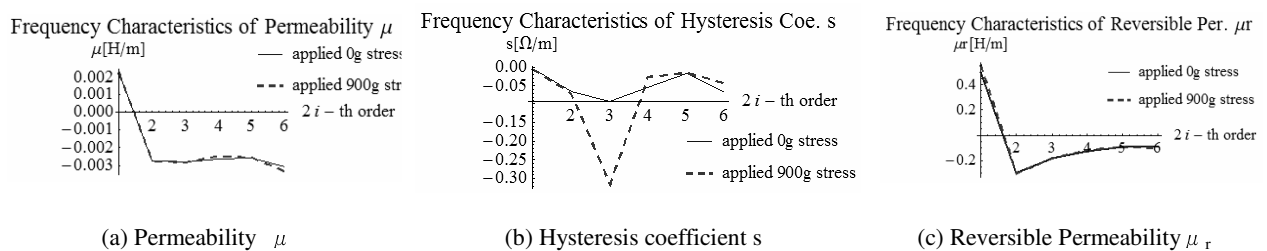


Fig 9. Parameters μ , s , and μ_r values to each of the harmonics when impressing high exciting voltage.

Figures 7-9 show the parameters μ , s , and μ_r values to each of the harmonics when impressing the low, middle and high exciting voltages. According to the variation of s shown in Figs. 7(b), 8(b), 9(b), it is found that the parameter s is highly sensitive to the applied stress.

Observe the hysteresis coefficient s in Figs. 7-9, it is obvious that the hysteresis parameter s greatly depends on the externally impressed stress while the other parameters μ , μ_r are keeping the similar values independent to the stress. This means that the hysteresis loss becomes larger in values when keeping the same magnetic flux density.

Thus, the external stress gives a large effect to the magnetic hysteresis, i.e., iron loss may be greatly increased by the externally applied stress.

4. Conclusion

The hysteretic nonlinear problems in ferromagnetic fields could be solved by means of the harmonic balance approach. The parameters μ , μ_r and s in the domain based model could be determined in each of the harmonics by the Fourier approach.

According to our approach, it has been revealed that the parameter representing the hysteretic property of the domain based model is highly sensitive to the applied stress. Namely, the iron loss in the electrical machines distributes depending on the stress distribution and may take the large in value at the highly stressed positions.

Design of the electrical machines essentially requires the efficiency item, which is directly related to the iron loss, because about 60% in the entire loss is the iron loss. In particular, thermal design of the electrical machines requires the exact iron loss distribution to work out the compact high power electrical machines.

References

- [1] Y.Saito, K.Fukushima, S.Hayano and N.Tsuya, Application of a Chua type model to the loss and skin effect calculations, *IEEE Transaction on Magnetics*, Vol.MAG-23, No.5, pp.2227-2229, Sep.,1987.
- [2] Y.Saito, Y.Kishino, K.Fukushima, S.Hayano and N.Tsuya, Modelling of magnetization characteristics and faster magnetodynamic field computation, *Journal of Applied Physics*, Vol.63, No.8, pp.3174-3178, Apr., 1988.
- [3] S.Hayano, Y.Saito, and Y.Sakaki, A magnetization model for computational magnetodynamics, *Journal of Applied Physics*, Vol.29, No.28, pp.4614-4616, Apr., 1991.
- [4] A. Ktena, and E.Hristoforou, Stress Dependent Magnetization and Vector Preisach Modeling in Low Carbon Steels, *IEEE Transactions on Magnetics*, Vol.48, No.4, pp.1433-1436, Apr.,2012.
- [5] P.Vourna, A. Ktena, and E.Hristoforou, Residual Stress Analysis in Nonoriented Electrical Steel Sheets by Barkhausen Noise Measurements, *IEEE Transactions on Magnetics*, Vol.50, No.4, pp.1-4, Apr.,2014.
- [6] A. Ktena, C. Manasis and E.Hristoforou, On the Measurement of Permeability and Magnetostriction in Ribbons and Wires, *IEEE Transactions on Magnetics*, Vol.50, No.4, pp.1-4, Apr.,2014.
- [7] Jawad Faiz, Behrooz Rezaeealam, and Sotoshi Yamada, Coupled finite element boundary element analysis of a reciprocating self-excited induction generator in a harmonic domain, *IEEE Transactions on Magnetics*, Vol.41, No.11, pp.4250-4256, Nov.,2005.
- [8] Jun Wei Lu, Sotoshi Yamada, and H. Barry Harrison, Application of harmonic balance-finite element method (HBFEM) in the design of switching power supplies, *IEEE Transaction on Power Electronics*, Vol.11, No.2, pp.347-355, Mar.,1996.
- [9] J.Lu, S.Yamada, K.Bessho, Time-periodic magnetic field analysis with saturation and hysteresis characteristics by harmonic balance finite element method, *IEEE Transaction on Magnetics*, Vol.26, No.2, pp.995-998, Mar.,1990.
- [10] J. Lu, S.Yamada, and H. Harrison, A parallel-computation model for nonlinear electromagnetic field analysis by harmonic balance finite element method, *IEEE First International Conference*, Vol.2, pp.780-787, Apr.,1995.

Field Test of the Backside Defect Searching by Low Frequency Excitation of the ∞ Coil

Shunichi HAMANAKA^{1,*}, Iliana MARINOVA², Yoshifuru SAITO^{1,†}, Manabu OHUCH³, Hideo MOGI³, and Yoshiro OIKAWA³

¹ Graduate School of Electrical Engineering, Hosei University, Tokyo 184-8584, Japan

² Technical University of Sofia 1756, Bulgaria

³ Emic (Denshijiki Industry) Co., Ltd, Tokyo 115-0051, Japan

ABSTRACT

Previously, we have proposed a ∞ coil as a high sensibility eddy current testing (ECT) sensor. This paper reports the liftoff characteristics of backside defect searching under the practical factory environments when employing the low frequency excited ∞ coil. However, the low frequency ∞ coil excitation confronts to a noise problem in the practical field experiments. To overcome this difficulty, we employ the commercial based signal processing device "ET-5002" made by Emic (Denshijiki industry) Co., Ltd. As a result, we have elucidated that a liftoff characteristic of the backside defect searching is clarified by employing the low frequency excitation to our ∞ coil under the practical factory environments. Thus, the practical field test has confirmed our ∞ coil methodology.

KEYWORDS

backside defect searching, eddy current, nondestructive testing, ∞ coil

Article history:

Received # Month Year

Accepted # Month Year

1. Introduction

The modern engineering products such as air-plane, automobile, smart building, high speed train and so on are essentially composed of the metallic materials for forming the shape of product, suspending the mechanical structure and constructing the frames.

In particular, the mass transportation vehicles, e.g. large air plane, high-speed train, express highway bus, carrying a large number of people are required the ultimate high safety as well as reliability. To keep the high safety and reliability, nondestructive testing to metallic materials is one of the most important key maintenance technologies because most of the frame materials are composed of the metallic materials.

Various nondestructive testing methods, such as eddy current testing (ECT), electric potential, ultrasonic imaging and x-ray tomography methods are currently used to modern airplane, high-speed-train and express high bus maintenance. Among these methods, ECT does not need complex electronic circuits and direct contact to the targets. Also, most of the targets whose major frame parts are composed of conductive metallic materials can be selectively inspected by ECT [1-6].

Operating principle of ECT is fundamentally based on a detection of the magnetic field distribution change due to the defect in the targets. To realize this principle, we have two methodologies. One detects the defect in the target as a change of input impedance of the exciting coil. This is because the magnetic field distribution is changed by the detour eddy currents flowing around the defect in the target which corresponds to the secondary circuit of a single phase transformer [5,6]. The other ECT sensor equips a sensing coil to detect the magnetic field change caused by the detour eddy currents flowing around the defect. The former and latter are called the impedance sensing and sensing coil types, respectively.

The sensing coil type is further classified into two variations. Most popular sensing coil type employs a spatial differential coil. This spatial differential coil detects the uniformity of the magnetic field distribution. Also the other type sets the sensing coil surface perpendicularly to those of the

* Corresponding author, Shunichi HAMANAKA, E-mail: shunichi.hamanaka.jc@stu.hosei.ac.jp

† Present address : c/o Y.Saito Lab., Graduate School of Electronics and Electrical Engineering Hosei university 3-7-2 Kajino Koganei 184-8584, Japan

exciting coil. This type detects only the magnetic fields caused by the detour eddy currents due to the defect in the target, because the sensing coil surface is perpendicularly set to those of the exciting coils.

When an alternating exciting current is flowing in the two adjacent circular exciting coils having a shape of ∞ character as shown in Fig.1, one and the other coils alternatively become the north and south magnetic poles. Also an alternating exciting magnetic flux flows through both surface of the two circular coils. A sensing circular coil wound in a parallel direction to the exciting magnetic flux path never induce any signals due to the exciting magnetic flux, i.e., the sensing coil whose coil surface is perpendicularly installed to that of two circular exciting coils as shown in Fig.1 detects only the magnetic fields caused by the detour eddy currents due to the defect in the target. This sensing probes is called the ∞ coils because of their exciting coil shape. For further details, see the reference [4] and a companion paper submitted to the ICSMT2014 by Maruyama et al.

Thus, our developed ∞ coil is one of the sensing coil types. Namely, the sensor used in this study detects only the magnetic fields caused by the detour eddy currents due to the defect in the target. When the detour eddy currents are caused by a backside defect of a sensing target, our ∞ coil detect the magnetic fields due to this eddy currents. This means that the backside defect in the target could be detected by the ∞ coil. One of the paramount importance characteristics is a liftoff characteristic between the surfaces of target and ∞ coil.

This paper tries to clarify the liftoff characteristic of the backside defect searching when employing a low frequency excited ∞ coil. As a result, it is revealed that the low frequency excited ∞ coil is capable of detecting the backside defects over 1mm liftoff while the measured signals are processed by the standard ECT signal processing device **ET-5002** made by Emic (Denshijiki industry) Co., Ltd., in Japan.

2. Experiments

A theoretical background of the low frequency exciting ECT greatly depends on the skin effects, i.e., low frequency magnetic fields is possible to induce the eddy currents at the deeper location of the target metallic materials. Even though the absolutely detective sensitivities become lower, the lower frequency excitation of ECT enables us to detect the defects located at the deeper or backside of the target metallic materials.

In our experiments, we have employed a test object which is a copper plate having 2mm thickness, 20cm length and 10cm width. But this copper plate has a line crack defect having 1mm depth from the backside surface and 2mm width at the center of backside as illustrated in Fig. 1.

Consideration of the skin depth, the absolute sensitivities and higher frequency noise signals accompanying the practical field measurements has led to employ the 2kHz as the best excitation frequency.

2.1. Liftoff characteristic simulation of the ∞ coil.

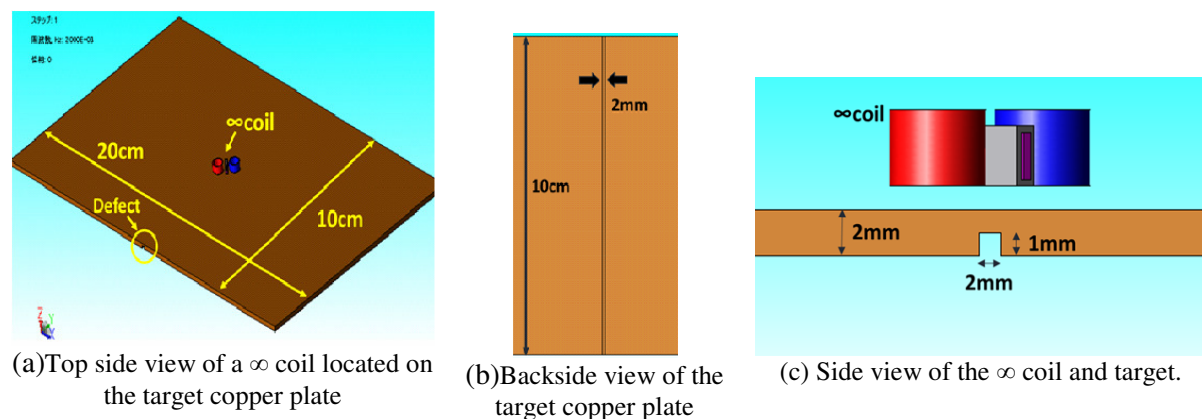


Fig. 1. Schematic diagram of the 3D FEM simulation

One of the distinct merits of ECT is that the ECT does not need direct contact to the target material. This means that the liftoff, i.e., a distance between the target and sensor surfaces, characteristic is of the paramount important factor for the ECT, because of the easiness of maintenance.

In the present paper, we have evaluated the liftoff characteristic of the low frequency excited ∞ coil when changing the liftoff distances from 0.07mm to 3mm under the practical factory conditions

Figure 1 shows a schematic diagram of the 3D finite elements simulations. Also, the practical liftoff measurement conditions are set as possible as the similar to that of the simulations. Table 1 lists the various parameters used in not only the computations but also experiments.

Table 1 Various parameters used for the simulation and experiment of the tested ∞ coil

Exciting coil	
Outer diameter of coil	2.2mm
Inner diameter of coil	1.8mm
Coil length	3.3mm
Number of turns	100
Input exciting sinusoidal voltage	100V _{RMS}
Frequency	2kHz
Sensing coil	
Outer diameter of coil	1.1mm×2.6mm
Inner diameter of coil	0.5mm×2mm
Coil length	4.8mm
Number of turns	100
Core material	Mn-Zn(Ferrite 3000)

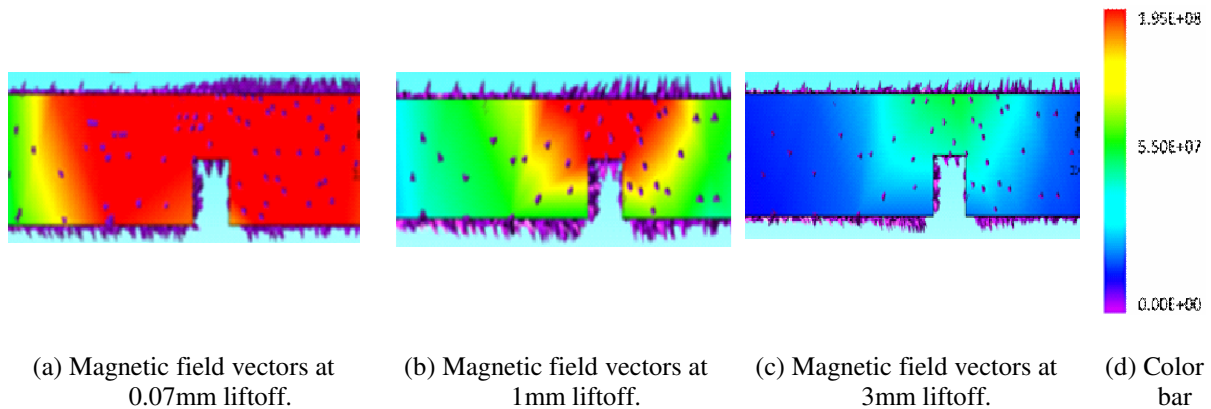


Fig.2. Magnetic fields and eddy currents distributions by the 3D FEM simulations. Color bar denotes the magnitude of eddy currents. Magnitude and direction of the magnetic field vectors are shown by the colors and triangular symbols, respectively.

Figures 2.(a)-(c) show the magnitude of eddy currents and magnetic field vector distributions when changing 0.07, 0.6, 1, 2 and 3mm liftoffs. In these figures, a color bar denotes the magnitude of the eddy currents. Also, the magnitude and direction of magnetic field vectors are denoted by the colors and triangular symbols, respectively.

The maximum magnitude of eddy current is obtained at the closest liftoff 0.07mm. Of course, the smallest magnitude of eddy current is obtained at the longest liftoff 3mm. This means that sensor sensitivity is inversely in proportion to the magnitude of liftoff.

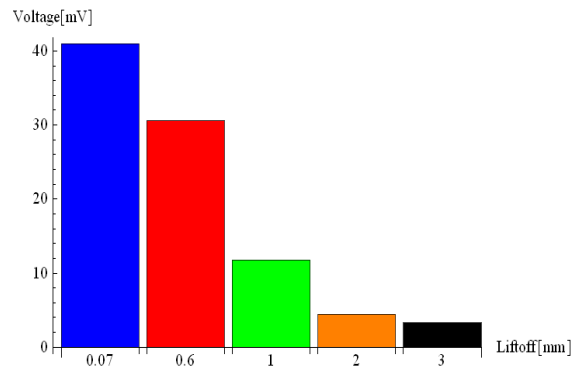


Fig.3. Liftoff characteristics in terms of the sensor induced peak voltages by the 3D FEM simulation.

When the line defect at the backside is located at 45 degree to a line connecting the centers of right and left exciting coils in the ∞ coil, the maximum sensor output voltage could be observed[4,5]. Thereby, all of the 3D finite elements simulations have been carried out at this maximum output condition. Figure 3 shows the peak values of the sensor output voltages when changing the liftoffs from 0.07mm to 3mm. According to the result in Fig. 3, it is found that the low frequency excitation ∞ coil makes it possible to detect the backside defect at the 3mm liftoff from the front surface of the target copper plate. Also, it is obvious that the sensor output voltage is inversely proportional to the liftoff distance.

2.2. Experimental Liftoff characteristics of the ∞ coil

2.2.1. Experiment

To examine the validity of the simulation results, the liftoff characteristic of the ∞ coil is measured under the practical factory conditions. Various parameters used in the experiments are listed in Table 1. Figure 4 shows the target test piece and the ∞ coil.

The target test piece having a line defect of the 2mm width and 1mm depth has been emulated by overlapping the two copper plates having 1mm thickness as shown in Figs.4(a) and 4(b). The pictures in Figs. 4(a), 4(b) show the top and backside views of the two copper plates emulating the target test copper plate, respectively.

Figure 4(c) shows the pictures of the ∞ coil used to the experiments. Specification of this sensor is the same as those of the simulated one.

The ∞ coil had been moved over the target surface with 50mm/s speed by a two-axis driven robot shown in Fig.5. In accordance with the movement, the sensor output signals are processed by the Japanese standard ECT signal processor "ET-5002" shown in Fig.6.

The ET-5002 signal processor makes is capable of amplifying and filtering functions of input the signals. We had employed 2kHz exciting frequency for the backside defect searching. The liftoff positions had been changed from 0.07mm to 3mm by controlling the 2-axes driven robot. The gain had been set to 60dB by the ET-5002. Also, the high and low pass filters had been set to the off and on at 10 Hz by the ET-5002, respectively.

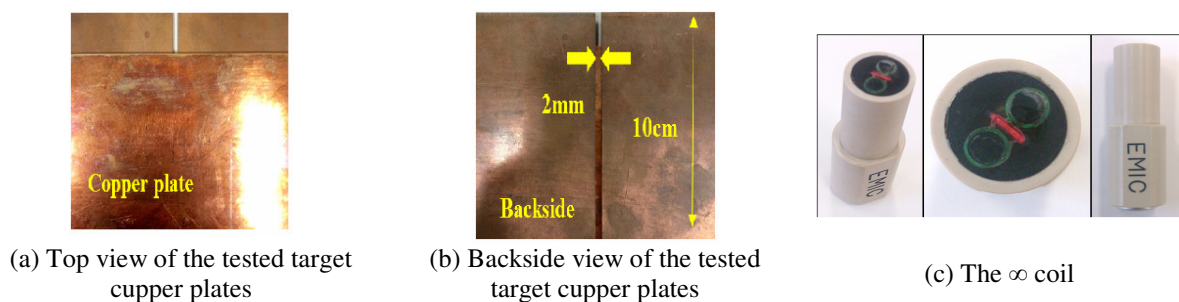


Fig.4.The tested target pieces and ∞ coil.



Fig.5. A two-axes driven robot for the sensor positioning.



Fig. 6. Japanese standard ECT signal processor "ET-5002" made by Emic (Denshijiki Industry) Co., Ltd.

2.2.2. Experimental results

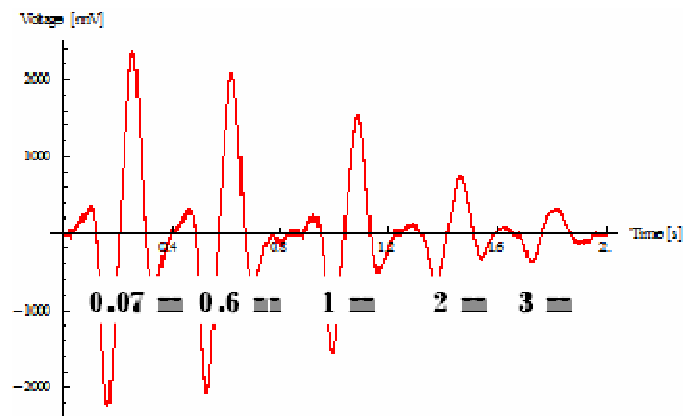


Fig.7. Sensor output signals processed by ET-5002 at the different liftoff magnitudes.

Figure 7 shows the sensor output signals when changing the liftoffs. These signals were processed by the ECT signal processor ET-5002 so that most of the environmental electromagnetic noise had been removed.

Observe the signals in Fig. 7 makes it possible to find the 5 distinct peaks in each of the liftoff positions. This suggests that the backside defect could be detected by the low frequency excited ∞ coil even though the longest 3mm liftoff. Further, the peak output signal at each of the liftoff positions is decreasing in proportional to the liftoff magnitudes. This relationship between the peak values of output signal and liftoff magnitudes takes the similar tendency to those of simulated one.

3. Comparison between the simulated and experimented results

Because of the signal processing by the ET-5002, it is difficult to compare the simulation and experiment results, directly. In addition, the 3D finite elements simulation had been carried under the ideal noiseless environments, even though the numerical round off as well as truncation errors could be neglected. The practical experiments had been carried out in the factory filled up by various electromagnetic noise caused by the electromagnetic devices such as switching power suppliers, power amplifiers and so on.

To compare the simulation and experiment results, each of the results is normalized to the values between the 1 to 0. Figure 8 shows the comparison between the normalized simulation and experimental results.

Observe the results in Fig. 8 reveals that practical experimental result exhibits higher sensibility compared with those of simulation one. This may be considered that the practical experimental condition was far different to those of the simulation neglecting the numerical error. Since there are a

lots of ferromagnetic parts such as the arms of robot, then these ferromagnetic parts work as one of the magnetic flux paths which enhances the sensitivity of the sensor ∞ coil.

In other words, the backside magnetic field information could be transmitted by the ferromagnetic parts in the tested factory. Global relationship between the liftoff and sensor output signal magnitudes in the practical field tests is similar to those of simulation one.

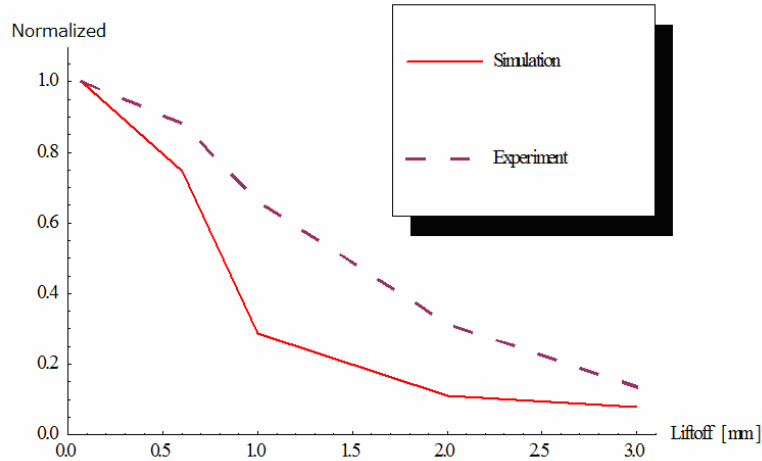


Fig.8. Comparison between the normalized simulation and experimental results.

Thus, we have verified the validity of 3D finite elements simulations. Also, we have succeeded in demonstrating the versatile capability of our ∞ coil by means of the low frequency excited ∞ coil for the backside defect searching.

4. Conclusion

In the present paper, we have evaluated the possibility of the backside defect searching by the low frequency excited ∞ coil.

As a result, it is revealed that the backside defects of target may be possible to detect by means of the low frequency excited ∞ coil. Also, the liftoff characteristic which is one of the most important characteristics in practical use has been elucidated in this paper.

References

- [1] S.Narishige, A.Nishimizu, M.Koike, Y.Abe, Y.Narumi, T.Tsuge, Improved Detection Performance using a Multi-frequency Method of Eddy Current Testing for Outside Circumferential Cracks near an Expansion of Heat Exchanger Tubes, *Non-Destructive Testing and Condition Monitoring*, Volume 52, Number 6, June 2010, pp. 298-301.
- [2] H.Hashizume, Y.Yamada; K.Miya, S.Toda, K.Morimoto, Y.Araki, K.Satake, N.Shimizu, Numerical and Experimental Analysis of Eddy Current Testing for a Tube with Cracks. *IEEE Trans. Magn.* 1992, 28, 1469-1472.
- [3] M.Morozov, G.Rubinacci, A.Tamburrino, S.Ventre, Numerical Models of Volumetric Insulating Cracks in Eddy-Current Testing with Experimental Validation, *IEEE Trans. Magn.* 2006, 42, 1568-1576.
- [4] Hiroki Kikuchihara, Iliana Marinova, Yoshifuru Saito, Manabu Ohuchi, Hideo Mogi and Yoshiro Oikawa, Optimization of the Eddy Current Testing, *Digest of The 15th Biennial IEEE Conference on Electromagnetic Field Computation*, Oita Japan November 11-14, WC4-4, PP.495. 2012.
- [5] Hiroki Kikuchihara, Yoshifuru Saito, Enhance the Sensibility of the ECT Sensor, *Journal of the Japan Society of Applied Electromagnetics and Mechanics*, Vol.21, No.3, 2013.
- [6] Kouki Maruyama, Iliana Marinova, and Yoshifuru Saito, Enhance the Sensibility of the Resonance type ECT Sensor, *JAPMED'8*, pp. 130-131, 2013.

A Study on Backside Defect Searching by Low Frequency Excitation of the ∞ Coil

Shunichi HAMANAKA ^{*1}, Yoshifuru SAITO ^{*1}, Iliana MARINOVA ^{*2}
Manabu OHUCHI ^{*3}, Hideo MOGI ^{*3} and Yoshiro OIKAWA ^{*3}

This paper describes a liftoff characteristic on backside defect searching by low frequency excitation of the ∞ coil. The low frequency ∞ coil excitation confronts to a noise problem in the practical experiments. To overcome this difficulty, this paper employs a Fourier transform signal processing method to remove the higher frequency noise components compared to the excitation one. Thus, we have succeeded in enhancing the S/N ratio and detecting the signals caused by the backside defects of the targets. As a result, we have elucidated that a liftoff characteristic of the backside defect searching is clarified by employing the low frequency excitation to our ∞ coil. Experimental as well as numerical verification along with intensive three-dimensional finite element method have been carried out to confirm our results.

Keywords: backside defect searching, eddy current, nondestructive testing, ∞ coil.

(Received: 24 July 2014, Revised: 23 April 2015, Revised: 22 May 2015)

1. Introduction

The modern engineering products such as air-plane, automobile, smart building, high speed train and so on are essentially composed of metallic materials for forming the shape of product, suspending the mechanical structure and constructing the structural frames.

In particular, the mass transportation vehicles, e.g. large air plane, high-speed train, express highway bus, carrying a large number of people are required the ultimate high safety as well as reliability.

To keep the high safety and reliability, nondestructive testing to the metallic materials is one of the most important key maintenance technologies, because most of the frame materials are composed of the metallic materials.

Various nondestructive testing methods, such as eddy current testing (ECT), electric potential, ultrasonic imaging and x-ray tomography methods are currently used to the modern airplane, high-speed-train and express high bus maintenance. Among these methods, ECT does not need complex electronic circuits and direct contact to the targets. Also, most of the targets, whose major frame parts are composed of conductive metallic materials, can be selectively inspected by ECT [1-3].

Operation principle of ECT is fundamentally based on the magnetic field distribution change detection due

to the defect in the targets. To realize this principle, we have two methodologies. One detects the defect in the target as a change of input impedance of the exciting coil. This is because the magnetic field distribution is changed by the detour eddy currents flowing around the defect in the target which corresponds to the secondary circuit of a single phase transformer [2-3]. In the other methodology, ECT sensor equips a sensing coil to detect the magnetic field change caused by the detour eddy currents flowing around the defect. The former and latter are called the impedance sensing and sensing coil types, respectively.

The sensing coil type is further classified into two variations. Most popular sensing coil type employs a differential coil, and also the other type sets the sensing coil surface perpendicularly to those of the exciting coil. As is well known the differential coil detects the uniformity of the magnetic field distribution. Similarly the perpendicularly installed sensing coil surface to those of exciting coil detects only the magnetic fields caused by the detour eddy currents due to the defect in the target.

Our developed ∞ coil is one of the latter types, i.e., detects only the magnetic fields caused by the detour eddy currents due to the defect in the target. A key idea of our ∞ coil is that the sensing coil wound around a ferrite bar is installed at the lowest magnetic field intensity region between the north and south poles of exciting coils, for further details see the references [1,2].

One of the most important targets of the non-destructive testing is the lift-off, i.e., distance between the target and sensor, because the lift-off characteristic indicates the sensing performance of the ECT sensor.

Further, backside defect searching is of paramount importance performance of the ECT, because only the ECT can detect the backside defects in a non-contacting manner.

Correspondence: S. HAMANAKA, Y.Saito Lab of Graduate school of electrical engineering, Hosei University, 3-7-2 Koganeicity Kazinocyou Tokyo 184-8584, Japan
email: shunichi.hamanaka.jc@stu.hosei.ac.jp

^{*1} Hosei University ^{*2} TU of Sofia ^{*3} Denshijilki Industry Co, Ltd

In the present paper, we try to evaluate the lift-off characteristic when searching for the backside defects by the low frequency exciting ∞ coil.

As a result, it is revealed that the low frequency ∞ coil excitation has made it possible to search for the backside defects even though the lift-off is 3mm distance.

At first, we describe the signal processing method accompanying the low frequency excitation of the ECT.

Second, we carry out the numerical as well as practical measurement tests. A 3 dimensional finite elements method (3D FEM) is employed as a tool of numerical test. Also, noisy signals accompanying the practical measurements are processed by Fourier transform method described in the 2nd chapter in this paper.

Finally, we conclude that it is possible to detect the backside defect even if the 3mm lift-off distance by our low frequency exciting ∞ coil method.

2. Signal processing method

2.1 Fourier transform method

One of the methodologies to remove the higher frequency noise components from the measured signal is the Fourier transform method.

Employ the Fourier transform approach makes it possible to pick up only the same frequency component of the exciting current.

3. Experiment

A theoretical background of the low frequency exciting ECT greatly depends on the skin effects, i.e., low frequency magnetic fields is possible to induce the eddy currents at the deeper location of the target metallic materials. Even though the absolute detect sensibilities become lower, the lower frequency excitation of ECT enables us to detect the defects located at the deeper or backside of the target metallic materials.

In our experiments, we have employed the two laminated copper plates, the upper is the normal copper plate having 2 mm thickness, 10 cm length, 2 mm width, and the backside is a target defect having a 1 mm line crack.

Consideration of the skin depth, the absolute sensibility and higher frequency noise signals accompanying the practical measurements have led to employ the 2 kHz as the best excitation frequency.

3.1 Lift-off characteristic of ∞ coil (Simulation)

One of the distinct merits of ECT is that the ECT does not need direct contact to the target material. This means that the lift-off, i.e. a distance between the surfaces of target and sensing coil, characteristic is of paramount importance in the ECT characteristics.

In the present paper, we have carried out the practical experiments as well as 3D numerical simulations concerning with the lift-off characteristic. Apply the low

frequency excitation to our developed ECT sensor named as ∞ coil yields the lift-off characteristic when changing the lift-off distances from 0.05 mm to 3 mm.

Figure 1 shows a schematic diagram of the 3D finite elements simulations. Also, the practical lift-off measurement conditions are set as possible as the similar to that of the simulations. Table 1 lists the various parameters used in the simulations.

Figure 2 shows the simulation results of the lift-off characteristic. Namely, Fig. 2 is the relationships concerning on the detected induced peak voltages and the lift-off distances. Each of the induced voltages at the five different lift-off distances suggests the backside defect in the target. Also, it is revealed that the induced voltage is inversely proportional to the lift-off distance.

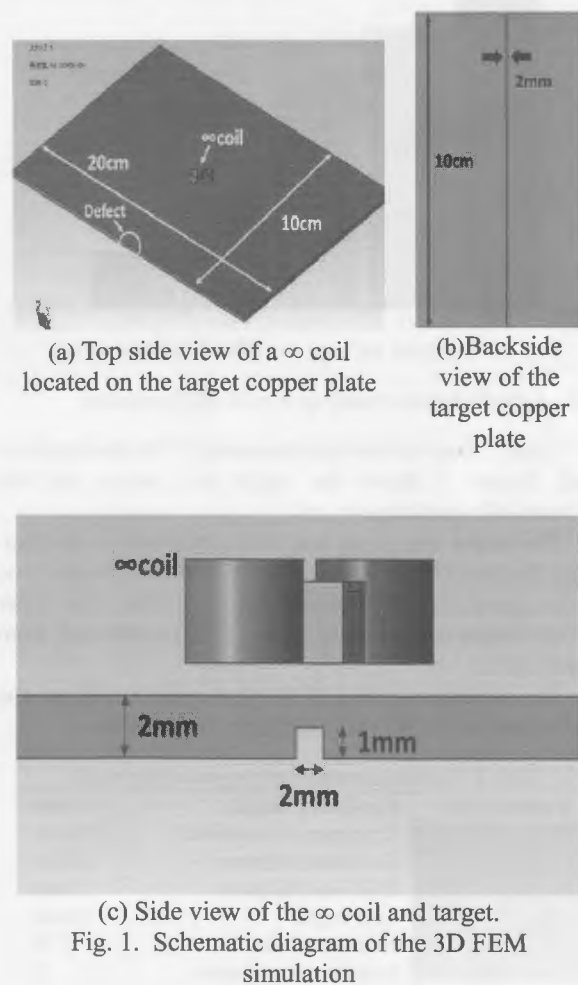


Fig. 1. Schematic diagram of the 3D FEM simulation

Table 1 Various constants of the tested ∞ coil

Exciting coil	
Coil outer diameter	22.4 mm
Coil inner diameter	20 mm
Coil length	10 mm
Number of turns	75
Input voltage (peak)	3 V
Frequency	2 kHz
Sensing coil	
Coil outer diameter	0.9 mm×2.4 mm
Coil inner diameter	0.5 mm×2.0 mm
Coil length	6.0 mm
Number of turns	100
Axis core	Mn-Zn ferrite 3000

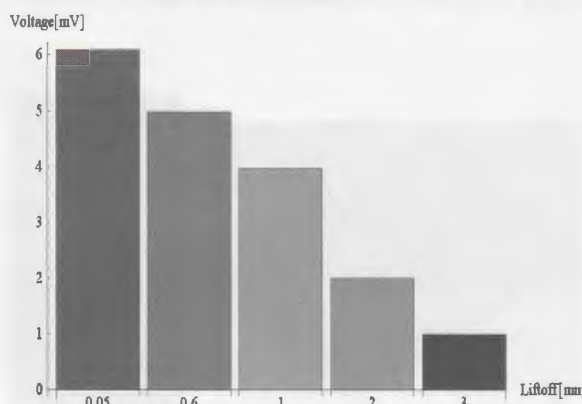


Fig. 2. Induced voltage vs. lift-off (simulation)

3.2 Lift-off characteristic of ∞ coil (Experiment)

Table 2 lists the various constants of the prototype ∞ coil. Figure 3 shows the target test pieces and the pictures of a prototype ∞ coil.

The target test piece has been emulated by overlapping the two copper plates having 1mm thickness. One is the upper copper plate without any defect. The other is the bottom copper plate having 2mm width and 1mm depth defect.

The various constant of the prototype ∞ coil are the same used in the 3D finite element simulations.

Table 2 Various constants of the prototype ∞ coil

Exciting coil	
	Conductor length 4.7mm
	Diameter of conductor 0.4mm
	Coil outer diameter 23mm
	Coil inner diameter 20mm
	Coil length 10mm
	Number of turn 75
	Number of col layers 3
	Number of coils 2
Sensing coil	
	Conductor length 60cm
	Diameter of conductor 0.1mm
	Axis core Ferrite bar (MnZn)
	Coil outer diameter 4mm×2.4mm
	Coil inner diameter 4mm×1.4mm
	Coil length 6.0mm
	Number of turn 100
	Number of coil layers 2



(a) Target test pieces



(b) Prototype of the ∞ coil

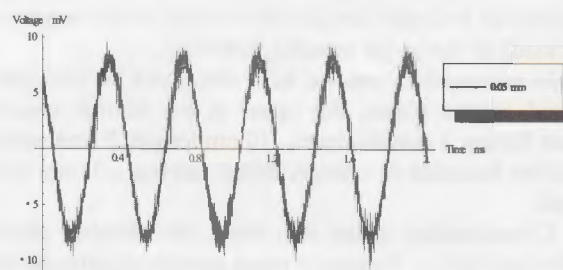
Fig. 3. The target tested piece and ∞ coil

Figures 4 (a)-(e) show the result of experiments. Observe these results shows that the detected signal includes a lot of high frequency noise caused by the experimental environments.

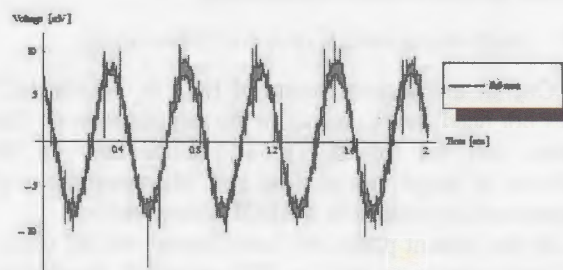
We could not see any defect on the front side of the target. Even though the high frequency noise, observe the same frequency components to those of the exciting currents in Fig. 4 suggests the backside defect of the target.

To remove the high frequency noise from the sensor output signals, we have employed the Fourier transform method. Since Fourier transform is able to decompose any waveforms into the higher harmonics, it is possible to pick up a particular frequency component from the measured signal. In our case, this particular frequency is the same as those of the exciting current.

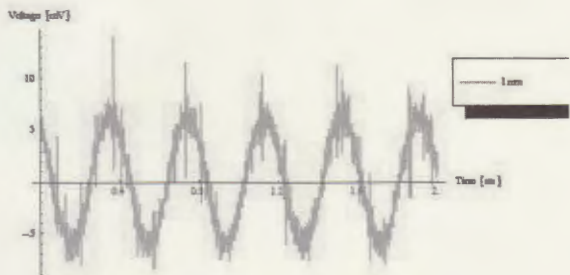
Figures 5 (a)-(e) show the induced voltage wave forms in the sensing coil after removing the higher frequency noise components by Fourier transform method from the Figs. 4 (a)-(e).



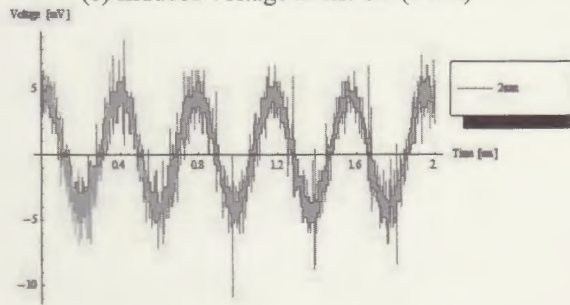
(a) Induced voltage in lift-off (0.05 mm)



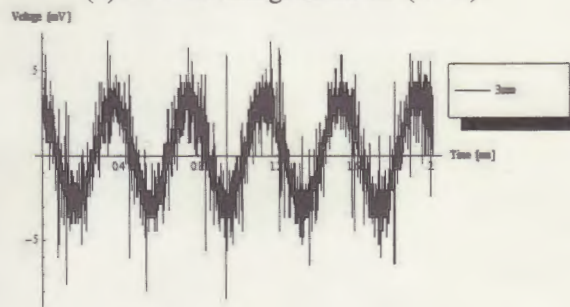
(b) Induced voltage in lift-off (0.6 mm)



(c) Induced voltage in lift-off (1mm)

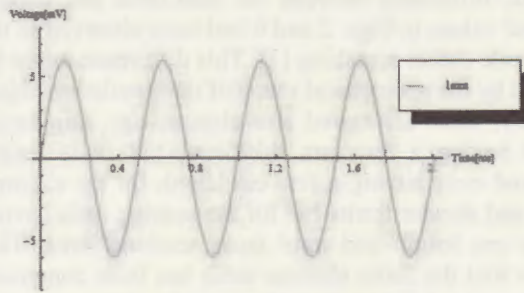


(d) Induced voltage in lift-off (2mm)

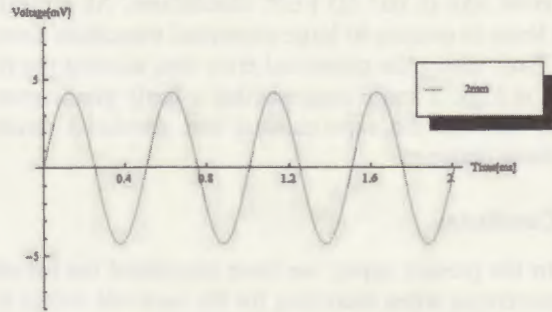


(e) Induced voltage in lift-off (3mm)

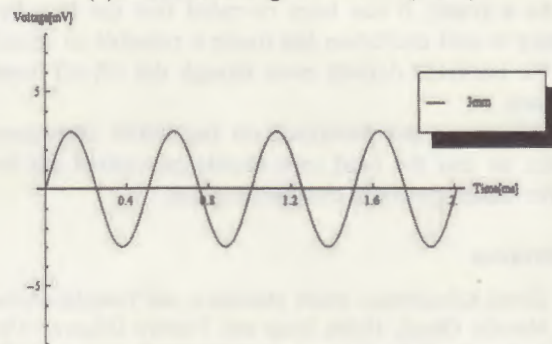
Fig. 4. Induced voltage waveforms when changing the lift-off distance.



(c) Induced voltage in lift-off (1mm)

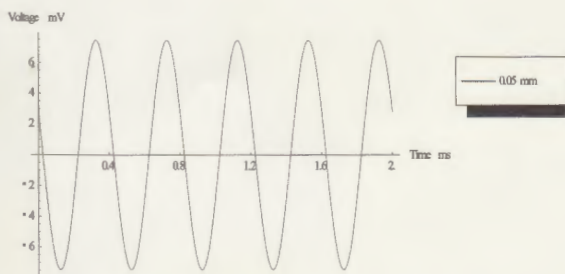


(d) Induced voltage in lift-off (2mm)

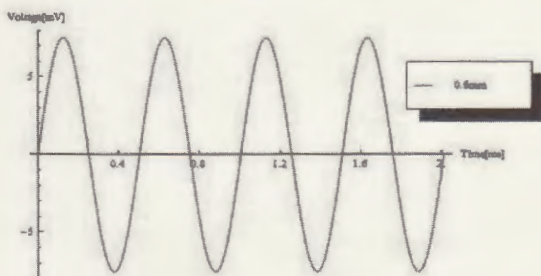


(e) Induced voltage in lift-off (3mm)

Fig. 5. Induced voltage waveforms after signal processing by Fourier transform method.



(a) Induced voltage in lift-off (0.05mm)



(b) Induced voltage in lift-off (0.6mm)

Figure 6 shows the experimentally obtained peak sensor output voltages having the same frequency to those of the exciting currents.

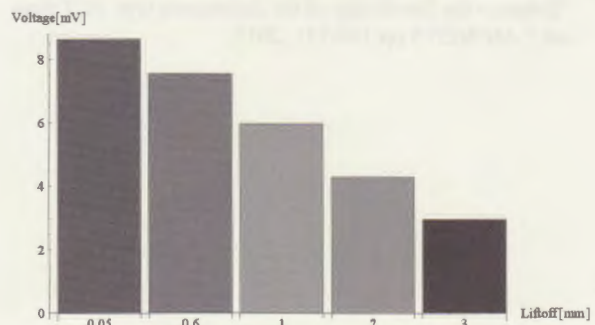


Fig. 6. Induced voltage vs. lift-off (Experiment)

The simulated peak voltage is somewhat smaller than these of measured one, however the sensing characteristic to the different lift-off distances is well corresponding to those of the simulation.

The difference between the simulated and experimented values in Figs. 2 and 6 had been observed in the front side defect searching [1]. This difference might be caused by the geometrical shape of the simulation object. Namely, there are mixed size objects, e.g., thin target metal having a few mm thickness, tall finite length solenoid coils having a few cm length for the exciting coils and slender ferrite bar for the sensing coils having a few cm length and mm^2 cross sectional area. This means that the finite element mesh has been composed of the mixed triangular elements having extremely different size in our 3D FEM simulations. As a result, this leads in essence to large numerical truncation errors.

Thus, taking the numerical error into account the results in Figs. 2 and 6 suggests that a fairly good agreement between the experimented and simulated results has been obtained.

4. Conclusion

In the present paper, we have elucidated the lift-off characteristic when searching for the backside defect by the low frequency exciting ∞ coil.

As a result, it has been revealed that the low frequency ∞ coil excitation has made it possible to search for the backside defects even though the lift-off 3mm distance.

This paper has described on the initial laboratory works, so that the field tests should be carried out for further development to the practical use.

References

- [1] Hiroki Kikuchihara, Iliana Marinova, and Yoshifuru Saito, Manabu Ohuch, Hideo Mogi and Yoshiro Oikawa, "Optimization of the Eddy Current Testing," *Digest of The 15th Biennial IEEE Conference on Electromagnetic Field Computation WC4-4* pp.495, Oita Japan November 11-14 2012.
- [2] Hiroki Kikuchihara and Yoshifuru Saito, "Enhance the Sensibility of the ECT Sensor," *Journal of the Japan Society of Applied Electromagnetics and Mechanics*, Vol.21, No.3, 2013.
- [3] Kouki Maruyama, Iliana Marinova, and Yoshifuru Saito, "Enhance the Sensibility of the Resonance type ECT Sensor," *JAPMED'8* pp.130-131, 2013.

The 17th International Symposium on
Applied Electromagnetics and Mechanics
(ISEM 2015)

Program Booklet

Awaji Yumebutai International Conference Center
Awaji City, Hyogo, Japan
15-18 September, 2015

<http://www.org.kobe-u.ac.jp/ise2015/home.html>

Hosted by
ISEM 2015 Organizing Committee

Supported by
The Japan Society of Applied Electromagnetics and Mechanics, and
Japan Society of Maintenology

Sponsored by
Tateisi Science and Technology Foundation,
Tsutomu Nakauchi Convention Foundation,
Hyogo International Association, and
Organization of Advanced Science and Technology, Kobe University

Flat/Film Infinity Coils and Backside Defect Searching

Shunichi HAMANAKA, Yoshifuru SAITO

*Graduate School of Electrical and Electronics Engineering, Hosei University, 3-7-2 Kajinotyo
Koganei, 184-8584, Tokyo, Japan*

Iliana MARINOVA

Technical University of Sofia 1756, Sofia, Bulgaria

Manabu OHUCH, Takaharu KOJIMA

EMIC (Denshijilki Industry) Co, Ltd, 115-0051, Tokyo, Japan

Abstract. Previously, we have proposed an infinity coil as a high sensibility ECT sensor. This paper has evaluated a possibility of the backside defect searching by the low frequency excitation of a modified infinity coil whose exciting coils are the flat/film shape to adapt to the curved test targets.

In the present paper, we have elucidated the liftoff characteristics of the backside defect searching when employing the low frequency excitation to our flat/film shape infinity coil.

1 Introduction

The modern mass transportation vehicles, e.g. air plane, high-speed train, carrying a large number of people are required the ultimate highest safety as well as reliability.

To keep the highest safety and reliability, nondestructive testing is one of the most important key maintenance technologies, because most of the frame materials are composed of metallic materials.

Operating principle of ECT is fundamentally based on the detection of magnetic field distribution change due to the defect in the targets. To realize this principle, we have two methodologies. One detects the defect in the target as a change of input impedance of the exciting coil. This is because the magnetic field distribution is changed by the detour eddy currents flowing around the defect in the target which corresponds to the secondary circuit of a single phase transformer [1-3]. The other ECT sensor equips a sensing coil in addition to the exciting coils for detecting the magnetic field change caused by the detour eddy currents flowing around the defect. The former and latter are called the impedance sensing and sensing coil types, respectively.

The sensing coil type is further classified into two variations. Most popular sensing coil type employs a spatial differential coil, and also the other type whose surface of the sensing coil is perpendicularly installed to those of the exciting coil. As is well known the spatial differential coil detects the uniformity of the magnetic field distribution. Similarly the other type whose surface of sensing coil is perpendicularly installed to those of exciting coil detects only the magnetic fields caused by the detour eddy currents due to the defect in the target. Our developed flat/film shape infinity coil is one of the these types. A key idea of our flat/film shape infinity coil is that the sensing coil wound around a ferrite bar is installed at the lowest magnetic field intensity region between the north and south poles of exciting coils [1].

This paper tries to clarify the liftoff characteristics of the backside defect searching when employing a low frequency excitation to the flat/film shape infinity coil. As a result, it is revealed that the low frequency excited flat/film shape infinity coil is capable of detecting the backside defects over 1mm liftoff

2 Experiments



Fig. 1 Reference ECT signal processor "ET-5002" produced by EMIC Co. LTD.

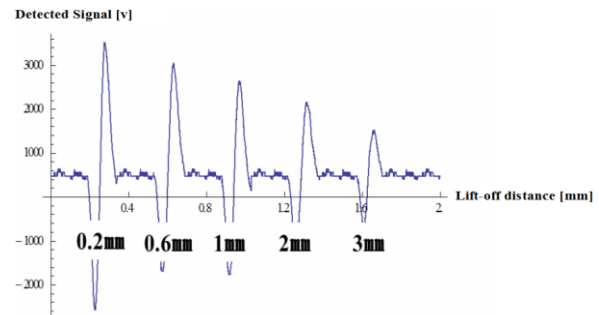


Fig. 2 Detected signal vs. Lift-off characteristic

In our experiments, we have employed the two laminated copper plates as a test target, the upper is the normal copper plate having 2mm thickness, 10cm length, 2cm width, and the backside is composed of 2 independent plates constructing a line crack having a 1mm depth and 2mm width.

Consideration of the skin depth, the absolute sensibility and higher frequency noise signals accompanying the practical measurements have led to employ the 2kHz as the best excitation frequency.

We measured the signals due to the backside defect by means of the commercial based signal processing device "ET-5002" shown in Fig1 while the flat/film shape infinity coil was scanned along a test target surface. Operating principle of the ET-5002 is that the equilibrium balanced condition of the bridge circuit picks up only the discontinuity of signals when the sensor scans over the defect. Lift-off distance was changed from 0.2mm to 3mm. The gain 60dB and 10Hz-256kHz band pass filter were set up to the ET-5002 for the backside defect searching.

Fig.2 shows detected signals by the flat/film infinity coil when scanning a surface of the target piece having a backside defect. Observe the detected signals makes it possible to find the 5 distinct peaks in each of the lift-off positions. Each of the detected signals at the five different lift-off positions suggests the existence of backside defect in the target piece. Also, it is found that the amplitude of the detected signals is inversely proportional to the lift-off distances.

3 Conclusion

In the present paper, we have employed the low frequency excitation of flat/film shape infinity coil to search for the backside defect of the metallic target when changing the lift-off distances from 0.2mm to 3mm. As a result, it has been clarified that the low frequency excitation of flat/film shape infinity coil makes it possible to search for the backside defects along with the signal processing device ET-5002 enhancing the S/N ratio.

References

- [1] Hiroki Kikuchihara, Iliana Marinova, Yoshifuru Saito, Manabu Ohuchi, Hideo Mogi and Yoshiro Oikawa, Optimization of the Eddy Current Testing, Digest of The 15th Biennial IEEE Conference on Electromagnetic Field Computation, Oita Japan November 11-14, WC4-4, PP.495. 2012.
- [2] Hiroki Kikuchihara, Yoshifuru Saito, Enhance the Sensibility of the ECT Sensor, Journal of the Japan Society of Applied Electromagnetics and Mechanics, Vol.21, No.3, 2013.
- [3] Kouki Maruyama, Iliana Marinova, and Yoshifuru Saito, Enhance the Sensibility of the Resonance type ECT Sensor, JAPMED'8, pp. 130-131, 2013.

Ingeniously Coil Connection and its Application to the Tesla Coils

Kazuya Okuda^{1, a}, Iliana Marinova^{2, b} and Yoshifuru Saito^{1, c}

¹c/o Y.Saito Lab., Graduate School of Electronics and Electrical Engineering,

Kajino Koganei, Tokyo 184-8584, Japan

²Dept. of Electrical Apparatus, Technical University of Sofia, 1756 Sofia, Bulgaria

^akazuya.okuda.2n@stu.hosei.ac.jp, ^biliana@tu-sofia.bg, ^cysaito@hosei.ac.jp

Abstract. This paper proposes a simple method to get the stabilized discharging characteristics by the Tesla coil without additional electronic circuits. Also, it is revealed that an ingenious coil connection changes the Tesla coil into a dramatically stable high voltage dischargeable source.

1. Introduction

Stable discharging is essential to the discharge machining, lighting, metal welding connection, and so on. The Tesla coil may be the oldest method generating high voltage source for discharging [1]. Further the Tesla coil may be regarded as one of the coreless transformer whose secondary induced voltage is extremely high. Apply a primal input source having one of the resonant frequencies of secondary coil makes it possible to generate a high secondary voltage. This secondary high voltage discharges from an externally attached electrode working as a resonant capacitor. However, its discharging characteristic is intermittently and not so stable. Thereby, this requires equipping the other electronics to obtain the stable and continuous discharge.

This paper proposes a simple method to get the stable discharging characteristics by the Tesla coil without additional electronic circuits, i.e., a simple ingenious connection of secondary circuits changes the Tesla coil into a dramatically stable discharge generator [2].

2. Resonant Tesla Coils

A typical conventional Tesla coil which is composed of the two coaxial finite length solenoid coils. The number of the outer primal and inner secondary coils are small and extremely large, respectively. Thereby, the Tesla coil is one of the coreless transformer whose transform ratio $a=N_1/N_2$ are extremely small, where N_1 and N_2 denote the number of turns of primal and secondary coils, respectively.

When a coupling between the primal and secondary coils through a common magnetic flux is high, it is possible to obtain a high secondary induced voltage. However, their coupling is very small so that the Tesla coil could not use as a normal voltage boost up transformer.

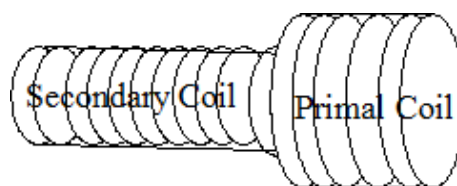


Fig.1 A typical Tesla coil

Fig. 2 shows a frequency characteristic of the secondary coil. Obviously, the secondary coil has the multiple resonant frequencies between the stray capacitance and leakage inductance. Thereby, it is essential to attach an external capacitor to fix a particular resonant frequency. After attaching the capacitor, it is possible to remove the effect of secondary leakage flux by the capacitor, i.e., a resonant phenomena, when supplying the resonant frequency to the primal coil. This leads to the desired high voltage determined by transformer ratio a .

On the other side, a resonant connection utilizing a capacitance between the inner and outer layer coils of the secondary winding exhibits a single resonant frequency characteristic as shown in Fig.2 [2]. A major resonant frequency in Fig. 2 is nearly 20MHz. On the contrary the single resonant frequency in Fig. 3 is nearly 30KHz. Difference between them is quite large frequency so that an ingeniously connection of the coils never requires an external resonant capacitor and creates the reasonable single resonant frequency characteristic.

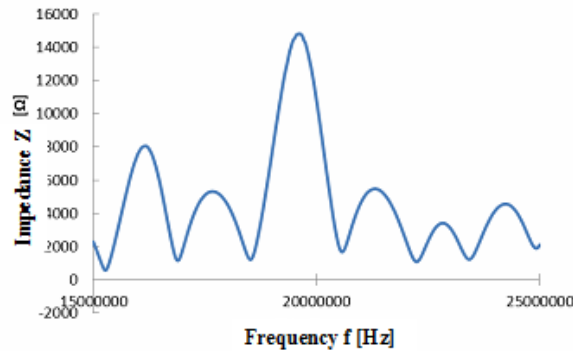


Fig.2 Frequency characteristic of the secondary coil.

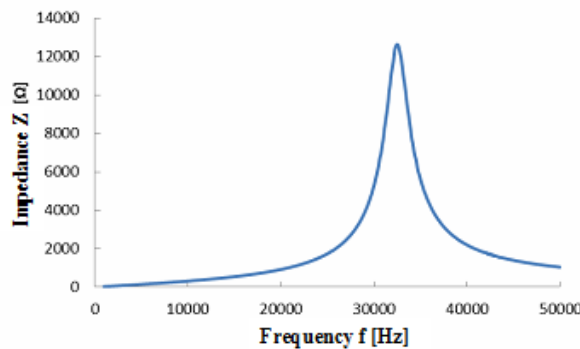


Fig.2 Frequency characteristic of the secondary coil when employing resonant connotation.

3. Conclusion

As shown above, we have succeeded in obtaining the single resonant frequency characteristic whose resonant frequency is relatively low. Thereby, it is possible to work out the devices, e.g., discharge machining, lighting, metal welding connection which require the stable discharging.

One of the innovative facts is that a simple ingeniously connection of the coils change the multi resonant into single resonant characteristics and removes the external electronic parts such as the external capacitor and high frequency processing elements.

References

- [1] <http://www.teslasociety.com/teslacoil.htm>
- [2] Y.Midorikawa, S.Hayano and Y.Saito, " A multi-resonant type inductor having notch filtering capability," IEEE Transaction on Magnetics, Vol.MAG-32, No.5,Sep.,1996,pp.4998-5000.

Design Strategy of The Practical Flat ∞ Coil

Takahiro Hyuga, N. Ishikawa, Yoshifuru SAITO

*Graduate School of Electrical and Electronics Engineering, Hosei University, 3-7-2 Kajino Koganei,
184-8584, Tokyo, Japan*

Iliana MARINOVA

Technical University of Sofia 1756, Sofia, Bulgaria

Manabu OHUCH, Takaharu KOJIMA

EMIC (Denshijilki Industry) Co, Ltd, 115-0051, Tokyo, Japan

Abstract. Previously, we had proposed an ∞ (infinity) coil for the high sensitive eddy current sensor and worked out several prototype of the ∞ coils. Because of the requirements of the practical environments, e.g., defects searching in the tight slits and curved surfaces, we have further developed the flexible flat/film ∞ coils.

In the present paper, consideration to the practical use to the design of prototype the flat/film ∞ coil lead an employment of the two semi-circle exciting coils. Experimental and 3D FEM simulations verify the validity of our practical design direction of the flat/film ∞ coil..

1 Introduction

Since most of the human products as well as infrastructures are mechanically supported by the iron or its composites, then nondestructive testing of metallic materials is of paramount important work to keep our daily life.

Previously we have succeeded in exploiting a new high sensibility eddy current testing (ECT) sensor called the ∞ coil [1]. Figure 1 shows one of the prototypes of our ∞ coil. Eventhough the developmens of the first trototype design was carrying out, strorong requirements to use the defect searching between the tight slit spaces because of the searching for the defects after assembles, and for the curved surfaces such as pipes.

To respond this requirement, we had exploited a flat ∞ coil [2]. Remarkably this new flat ∞ coil displayed a versatile capabilities for the defect searching caurved serface and high sensibility compared with the old one as shown in Fig.1.

This paper is concerning to decide the degin direction of the flat ∞ coil, e.g., cicular or square cross-section shape and the flat excaiting coils shoud be wound remaing or not emaing the cetrers of flat excaiting coils.

Finally, the first prototype degin direction of the flat ∞ coil is focused on the two key points, i.e, one is the shape of exciting coils, which enlarges the zero magnetic field region between the two adjacent coils constructing the north and south poles alternatively, and the second the shape of flat exciting coils whether each of the coils should be fully wound until no space or not fully wound remaining some space, namely each of the exciting coil surfaces does not has any area otherwise has a space enclosed by an exciting coil.



Fig. 1 The First Prototype of The ∞ coil.

2 Practical Prototype Design of ∞ Coil

Operating principle of original flat ∞ coil is that two adjacent coils constructing the north and south poles alternatively set a zero magnetic field region and keep this zero magnetic fields situation when eddy currents are flowing along the paths in parallel to the exciting coils. If the eddy currents could not flow the paths in parallel to the exciting coil on the test specimen, then a zero magnetic field region between the two exciting coil moves toward the other position. This means that a sensing coil located at a mid position of two exciting coil is possible to detect the disturbed magnetic fields, i.e., the defect in the test specimen could be detected from the sensing coil signal.

By means of the intensive 3D FEM simulation and experimental works, this paper reveals that the sensibility of the flat ∞ coil could be enhanced by enlarging the zero magnetic field region between the two adjacent exciting coils. This has been simply carried out by enlarging a two adjacent point to a two adjacent line. Effect of this exciting coil layout modification reflects on the output larger amplitude of sensing signals than those of conventional one. Also, we have carried out the 3D FEM simulations as well as experiments to the 10 turns coil having a space and the 20 turns having no space. Figure 2 shows the tested coils and their response signals to a straight line defects tilted 45 degree to the sensor coil of the ∞ coils.

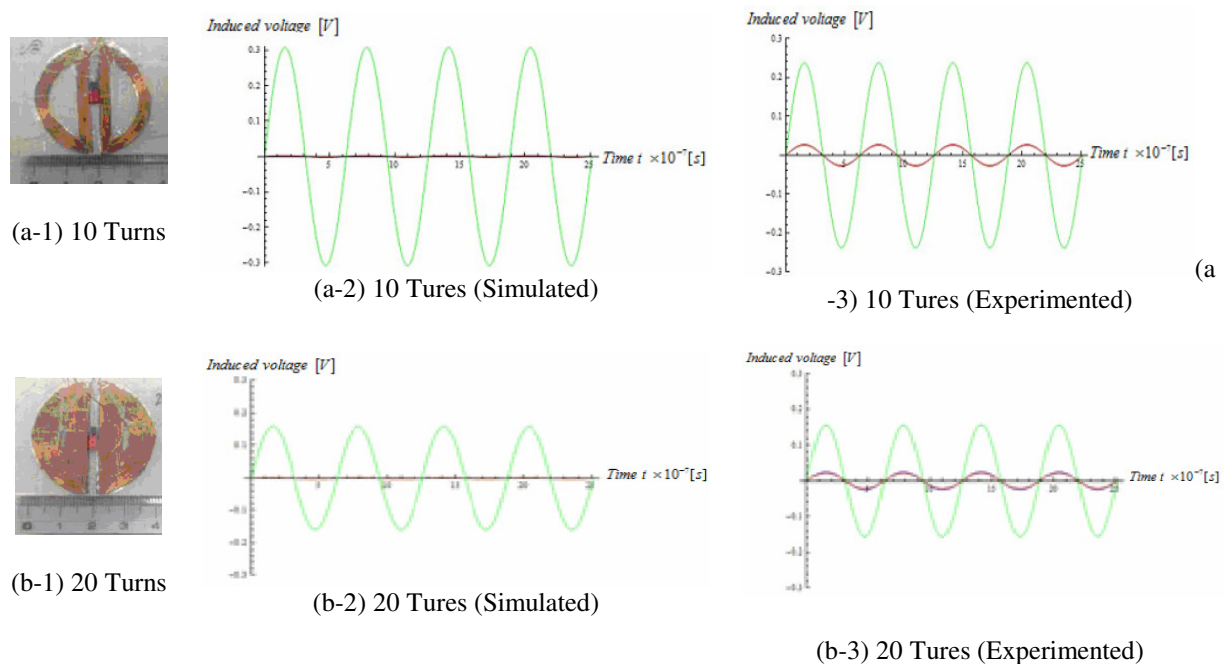


Fig. 2. The first tested flat ∞ coils.

The Green and Red lines are denoting the sensor output signals and noises, respectively.

As described above we have succeeded in decided to work out the first prototype design.

References

- [1] H. Kikuchihara et al, *Development of a New High Sensitive Eddy Current Sensor*, *Materials Science Forum* Vol. 792 (2014), 98-103.
- [2] K. Maruyama et al, *Developments of Flat ∞ Coil for Defect Searching in the Curved Surfaces*, *E-Journal of Advanced Maintenance*, in printing.

Frequency Fluctuation Signal Processing and Its Application to the Barkhausen Signals

Mirai IIDA, Yoshifuru SAITO

*Graduate School of Electrical and Electronics Engineering, Hosei University, 3-7-2 Kajinotyo
Koganei, 184-8584, Tokyo, Japan*

Iliana MARINOVA

Technical University of Sofia 1756, Sofia, Bulgaria

Abstract. Among a lot of signal processing methods, frequency fluctuation approach is rarely used. Only the $1/f$ frequency fluctuation is well known as a figure of healing activations. In the present paper, a generalized frequency fluctuation signal processing method is introduced to analyse the Barkhausen signals accompanying with the magnetization of the ferromagnetic materials. As a result, it is revealed that the situations of ferromagnetic materials under stressed or not are visualized in a three dimensional space.

1 Introduction

Barkhausen signal is observed in the ferromagnetic materials when they are magnetizing. It is well known that the Barkhausen signals are very sensitive to the physical external stress and radioactive damage to the ferromagnetic materials.

The iron and its composite ferromagnetic materials are widely used for main frame materials to support the mechanical structures in many artificial products and constructions. Because of their essential role, they are always got mechanical stress and they keep their past mechanical stress histories. Nondestructive detection of their mechanical stress as well as residual stress is of paramount importance for keeping the safety of the mechanical structures, since it is possible to see ahead of time what extent the mechanical structure will maintain their strength for further use.

The past researches concerning to a relationship between the Barkhausen signal and applied mechanical stress have revealed that Barkhausen signals are very sensitive to the mechanical stress and radioactive damage but any deterministic regularity has not been found [1,2]. Only a macroscopic regularity has been reported by means of a frequency fluctuation analysis approach [3]

This paper makes it possible to generalize 1^{st} order frequency fluctuation of the conventional analysis to the n^{th} order frequency fluctuation analysis. As a result, it is succeed in visualizing the specimen's situations under stressed or not stressed from their Barkhausen signals.

2 Generalized frequency fluctuation analysis

Conventional $1/f$ frequency analysis is that application of the 1st order least squares to the both Fourier power spectrum and frequency extracts the 1st order frequency fluctuation, i.e., Log of Fourier power spectrum is approximated by Log of $a_0 + a_1 f$, yields a 1^{st} order frequency fluctuation characteristic, where a_0 and a_1 are the 0^{th} and a 1^{st} order frequency fluctuation terms, respectively. If the frequency fluctuation term a_1 takes $a_1=1$, then we have the $1/f$ frequency fluctuation. One of the most famous frequency fluctuations is the $1/f$ frequency fluctuation, which can be observed in most of the natural phenomena such as natural wind, sea water waves, river flow sound and so on gives a healing effect to the mentalities via human sensibilities [4].

On the other side, we generalize this conventional 1^{st} order frequency fluctuation to the n^{th} order frequency fluctuation characteristics, i.e., Log of Fourier power spectrum is approximated by a Log of $a_0 + a_1f + a_2f^2 + \dots + a_n f^n$, where $a_0, a_1, a_2, \dots, a_n$ are the $0^{th}, 1^{st}, 2^{nd}, \dots, n^{th}$ order frequency fluctuation terms, respectively. Careful examination of the coefficients $a_0, a_1, a_2, \dots, a_n$ leads to the precise frequency fluctuation characteristic of the Barkhausen signals.

According to our experimental results, all of the frequency fluctuation characteristics are sufficiently represented up to the 4^{th} order terms. Fig.1 shows a typical relationship between the frequency characteristic and 4^{th} order least squares curve.

Let the normalized $1^{st}, 2^{nd}, 3^{rd}, 4^{th}$ order frequency fluctuation coefficients be respectively the coordinate values on the x-, y-, z-axes, and point shade color, then up to the 4^{th} order frequency fluctuation characteristics locate the three dimensional space coordinate position and point shade color.

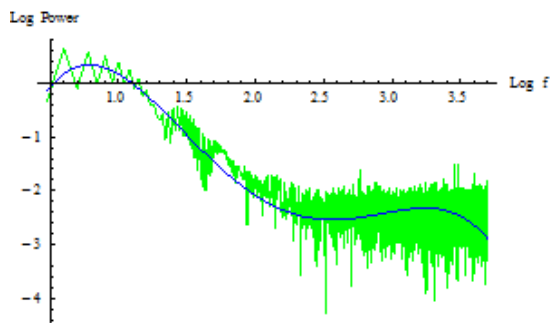


Fig. 1 A typical relationship between the frequency characteristic and 4th order least squares curve.

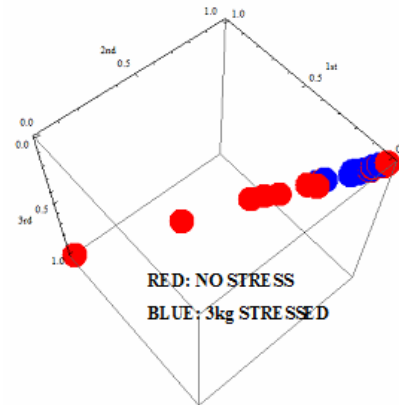


Fig. 2 The visualized stress situations by the 4th order frequency fluctuation analysis to the 30 specimens.

To check the validity of our approach, we have carried out the frequency fluctuation analysis to the 30 silicon steel sheet specimens when they are stressed and not stressed. Fig.2 shows the stress situations to the 30 silicon steel specimens. In Fig.2, the normalized $1^{st}, 2^{nd}, 3^{rd}, 4^{th}$ order frequency fluctuation coefficients are respectively the coordinate values on the x-, y-, z-axes, and point shade color. Comparison among the different specimens of this diagram visualizes an each of the distinct characteristics depending on their mechanical stress conditions.

3 Conclusion

As shown above, we have succeed in visualizing the stress situations of the silicon steel sheets in the 3 dimensional space whose coordinates are composed of the terms representing the higher order frequency fluctuation of their Barkhausen signals.

References

- [1] R M. Bozorth: Ferromagnetism, p. 462 (IEEE PRESS)
- [2] M. Katsumata, S. Hayano and Y. Saito: A Study of Barkhausen Phenomenon Visualization, *The Visualization Society of Japan*, B203, July, 2003.
- [3] S. Nojima and Y. Saito: Application of Frequency Fluctuation to Barkhausen Signals and its Application, *J. Magn. Soc. Jpn.*, 35, 380-385, 2011.
- [4] M. Teranishi, K. Maruyama, S. Hayano, and Y. Saito: Visualization of $1/f$ Frequency Component in Dynamic Image of Natural Phenomena, *The Visualization Society of Japan*, B108, July, 2005..

平面型 ∞ コイルの低周波励磁による裏面欠損探傷に関する -基礎リフトオフ特性-

濱中 峻一* 齋藤 兆古 (法政大学)

大内 学 児島 隆治 (電子磁気工業)

Backside defect searching by the low frequency excitation of a flat shape infinity ECT sensor coil
- Basic liftoff characteristics study-

Shunichi Hamanaka*, Yoshifuru Saito, (Hosei University)

Manabu Ohuch, Takaharu Kojima, (Denshijiki Industry Co, Ltd)

Previously, we have proposed a flat shape ∞ coil as a high sensibility ECT sensor. This paper has evaluated a liftoff characteristic to the backside defect searchings by the low frequency excitation of a flat shape ∞ coil. As a result, it is found that the low frequency excitation of a a flat shape ∞ coil promises its capability in particular to the lift of characteristics of the backside defect serachings in the target materials.

キーワード: 渦電流試験, 非破壊検査, 裏側欠損, 低周波励磁, ∞ コイル

(Keywords, ECT, nondestructive testing, backside defect, low frequency excitation, ∞ coil)

1. 序論

現代の文明社会を支えるのは人類の叡智が創造した多くの文明の利器による。例えば、高速な移動手段を提供する高速鉄道、自動車、航空機、そして、電力生成・系統システム、照明システム、セキュリティシステムなど、いわゆる産業プロダクトから鉄橋、大型ビルや高速道路などの社会的インフラストラクチャまで広汎で多岐に渡る文明の利器が存在し、人類の文明生活を支えているのは自明であろう。

産業プロダクトから社会的インフラストラクチャにいたる文明の利器の多くは何らかの形で機械的構造を持ち、強度や形状維持のフレームが存在する。機械的構造の強度を維持するフレームの多くは金属材料からなり、それぞれの産業プロダクトの機能を維持するため、機械的ストレスを受け続けている。

産業プロダクトの中で、人間の大量輸送に関わる大型バス、高速列車、大型旅客機のみならず原子力発電所で代表される大規模エネルギー変換システムなどのプラントや社会的インフラストラクチャ設備では、機械的ストレスだけでなく熱応力、中性子による劣化などがある。当然であるが、これらの産業プロダクトではフレームの健全性が高度な信頼性、安全性を確保するために極めて重要な要素である。

金属の健全性を確保する手段として最も基幹的で重要な技術が金属材料に対する非破壊検査技術である。金属の非破壊検査として、渦電流探傷法 (Eddy Current Testing, 以後、ECTと略記)、電気ポテンシャル法、超音波画像法およびX線断層撮影法のような様々な方法がある。この中で、金属の非破壊検査として、ECTによる方法は、検査対象と直接接触の必要がなく、比較的簡単な装置で高速な検査が可能である。このため、ECTは自動車を構成する膨大な数の部品検査から橋梁の劣化検査など極めて多くの分野で広汎に使われている。これは、人類の創造する文明の利器の力学的強度維持は大部分が導電性を有する金属材料からなるためであり、特にECTは選択的に非接触で金属部分のみ検査可能であることに拠る。さらにECTは、検査対象に非接触で探査可能であり、発振器、アンプ、探査プローブコイル、オシロスコープなど比較的安価で簡素な装置で構成可能であるため、最もメジャーな非破壊検査技術である。

本論文は、平面型 ∞ コイルを用いた平面及び曲面の裏面欠損探査で、主として被検査対象とセンサ間の距離、すなわち、リフトオフ特性に関する数値シミュレーションとその実験を行ったので報告する。

2. ∞ コイル

〈2.1〉 ECT センサの動作原理

ECTの動作原理は、大別して二方法ある。一方は交番磁界

を被検査対象に照射することで被検査対象中に渦電流を発生させ、被検査対象中の欠損の有無による渦電流分布の相違を電源から見た入力インピーダンスの変化で感知する方法である。ここでは、この ECT 法をインピーダンス感知型と呼ぶ。このインピーダンス感知型 ECT の特徴は励磁コイルがセンサも兼ねる点であり、構造が簡単で安価である。

他方は励磁コイルの他に独立した検出コイルを備えた励磁・検出コイル分離型である。この励磁・検出コイル分離型は被検査対象中の欠損の有無に起因する渦電流分布の相違が喚起する磁束の変化を感知する検出コイルの配置に自由度を持つ。このため、励磁・検出コイル分離型は、インピーダンス感知型に比較して高感度とされているが、検出コイルの構造や設置場所などに多くの経験的習熟度を必要とする。

本論文で採用する平面型 ∞ コイルの動作原理は励磁・検出コイル分離型である。

〈2・2〉 ∞ コイルの動作原理

∞ コイルの原理的な特徴は、 ∞ 文字状に巻かれた二個の励磁コイルに通電し、左右の励磁コイル下端に N 極と S 極の磁極を形成し、N 極と S 極の磁極の間には必ず存在するゼロ磁界領域に磁性体コアに巻いた検出コイルを配置する点にある。被検査対象が存在しない、もしくは被検査対象に欠損が存在しない場合、励磁コイルが生成する磁界強度分布の対象性が保たれるから、ゼロ磁界領域も維持され検出コイルには電圧は誘起しない。しかし、磁界強度分布の対象性が被検査対象中の欠損に起因して崩され、結果としてセンサコイルに誘起する電圧から欠損が感知される。

換言すれば、N 極と S 極間には必ずゼロ磁界領域が存在する。励磁コイルが生成する N 極と S 極の磁界強度分布が対象である限り、励磁コイル間のゼロ磁界領域は維持される。しかし、被検査対象に欠損があれば、欠損に起因する渦電流分布の非対称性に起因する磁界は検出コイルへ鎖交する。結果として検出コイルに電圧が誘起し欠損が探知される。

実際は、磁界がゼロとなる領域は限られた微小範囲であるため、検出コイル軸はゼロ領域へ平行に被検査対象面へ最も接近した位置へ配置する。すなわち、 ∞ 文字状の励磁コイル軸へ磁界が直交する方向へ検出コイルの軸を配置し、励磁コイルと検出コイル間の相互インダクタンスをゼロにする。両者に相互結合が起こるのは検査対象の欠損を通した場合のみとする。これが回路的な観点から見た ∞ コイルの動作原理である^{(1), (2)}。

〈2・3〉 ∞ コイルの低周波励磁

ECT の検査対象に対する磁束の表皮浸透深さは駆動周波数に依存性する。磁束の表皮浸透深さは駆動周波数の平方根に反比例するため、駆動周波数が数メガ Hz と比較的高い場合検査対象の深部まで浸透せず、欠損の表面のみしか渦電流が誘起されない。すなわち探査範囲が表面に限定される。

励磁周波数を低減することにより検査対象の深部まで磁

束が浸透し、渦電流が検査対象の深くまで誘起されるため、結果として検査対象の裏側の欠損探傷が可能と考えられる。

〈2・4〉 表皮浸透深さ

表皮浸透深さ d は以下のように定義される。

$$d = \sqrt{\frac{2}{\omega\mu\sigma}} \dots\dots\dots(1)$$

ここで、被検査対象の比透磁率は 1 とし、式(1)のパラメータは以下の通りである。

ω : $2\pi f$,

f : 周波数 [Hz],

μ : 真空中の透磁率 $4\pi \times 10^{-7}$ [Hm],

σ : 導電率 [S/m]

電流は表面から内部に浸透するに従い $e^{-x/d}$ の形で減少する。表面から内部への浸透深さ $x = d$ の点での電流が表面の値が $1/e$ になる。この d が表皮浸透深さと呼ばれる⁽³⁾。

3. 平面状対象の裏面欠損探査実験

〈3・1〉 シミュレーションに依るリフトオフ特性

リフトオフとは、ECT センサと被検査対象間の距離である。リフトオフ特性は検出感度とリフトオフ距離の関係であり、リフトオフ距離が ECT として最も重要な特性であることは自明である。

本論文では、リフトオフを 0.2mm から 3mm まで変化した場合のセンサ出力特性を吟味する。

被検査対象は厚さ 2mm の銅板からなり、裏面に幅 2mm、深さ 1mm の直線状欠損が存在する。図 1 は、三次元有限要素法のシミュレーションモデルを示し、表 1 は、励磁コイルと検出コイル、それぞれの諸定数を示す。

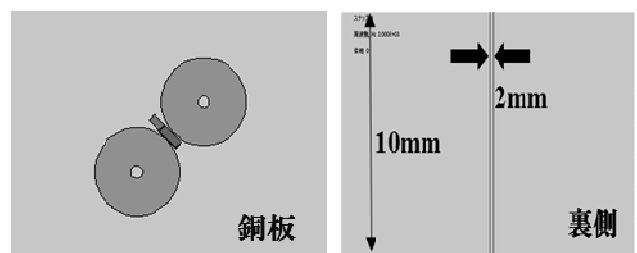


図 1 三次元有限要素シミュレーションの概略図
Fig. 1. Schematic diagram of the 3D FEM simulation

リフトオフを 0.2mm から 3mm まで変化した場合のシミュレーション結果を述べる。

励磁周波数を 2kHz とした場合、表皮浸透深さは(1)式より

$$d = 1.477[\text{mm}]$$

となる。

よって、深さ 1mm 以上の深さに存在する裏側欠損探傷が可能であると考ええる。

表 1 平面型 ∞ コイルの諸定数 (シミュレーション)

励磁コイル	
外径	22mm
内径	3.0mm
長さ	10mm
巻数	20mm
入力電圧	3.0V
周波数	2kHz
検出コイル	
外径	0.9mm×2.4mm
内径	0.5mm×2mm
長さ	6mm
巻数	100
磁性体コア	Mn-Zn_ferrite_300

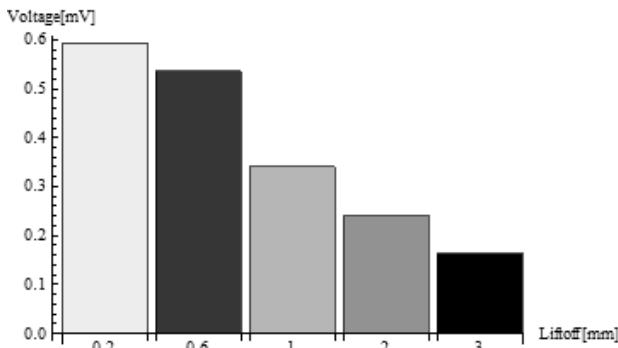


図 2 シミュレーションによる
センサピーク電圧とリフトオフの関係

Fig. 2. Induced voltage vs. lift-off

∞ コイルの探査感度、すなわち、直線状欠損による渦電流の乱れが検出コイルの電圧を最大とする場合は、直線状欠損が検出コイル軸に対して 45 度である場合であり、全てのシミュレーションは上記の最大感度条件で行った。

図 2 の有限要素法に拠るシミュレーション結果は、リフトオフを 0.2mm から 3mm に変更した場合の検出コイルのピーク誘起電圧とリフトオフの関係を示す。

図 2 のシミュレーション結果は、リフトオフを 0.2mm から 3mm まで不規則な間隔で 5 点変更した場合、センサピーク誘起電圧はリフトオフに対して反比例する傾向が伺える。すなわち、リフトオフが大きくなればセンサピーク誘起電圧は減少する。

図 2 で、センサピーク誘起電圧は、リフトオフ 0.2、0.6、1、2、さらに 3mm に対してそれぞれ 6.09、4.98、3.96、2.0、0.994mV である。

〈3・2〉リフトオフ特性の実験

〈3・2・1〉実験方法

シミュレーション結果の妥当性をしらべるため、表 1 の仕様で作成された諸定数の試作平面型 ∞ コイルのリフトオフ特性を実際に測定する。測定に使用した被検査対象であ

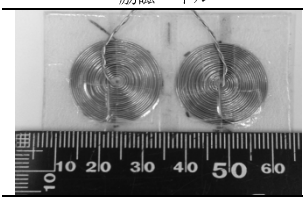
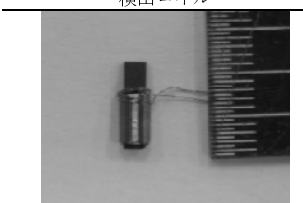
る銅板と試作 ∞ コイルを図 3 に示す。

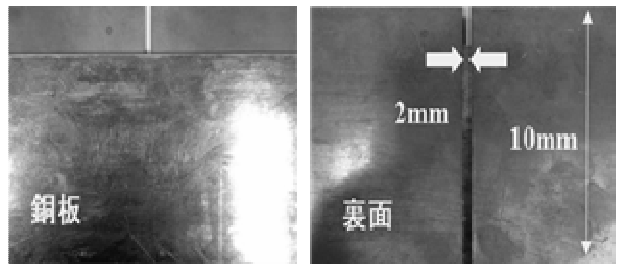
図 3(a)に示す被検査対象中の幅 2mm、深さ 1mm の直線状欠損は幅 2mm の銅板の裏面に厚さ 1mm の無欠損な銅板 2 枚を 2mm の間隔を空けて重ねることで模擬した。

図 3(b)に示す試作 ∞ コイルは 2 個の励磁コイルと 1 個の検出コイルからなり、諸定数はシミュレーションで用いた図 1 のそれらと同一である。

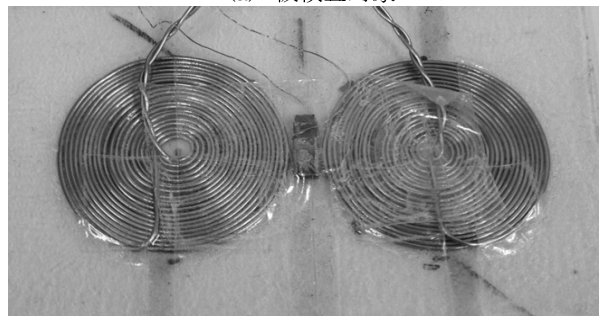
表 2 試作平面型 ∞ コイルの諸定数

Table.2. Various constants of the flat shape of prototype ∞ coil

励磁コイル		コイル長	0.4mm
		外径	22mm
		内径	3.0mm
		巻数	20
		コイルの数	2
		入力電圧	3V
		励磁周波数	2kHz
検出コイル		導体長	60cm
		導体の直径	0.1mm
		磁性体コア	Ferrite bar(MnZn)
		外径	2.4mm×2.4mm
		内径	1.4mm×1.4mm
		コイル長	6mm
		巻数	100
		コイル層の数	2
		コイルの数	1



(a) 被検査対象



(b) 試作平面型 ∞ コイル

図 3 検査対象と試作 ∞ コイル

Fig.3. The target tested piece and flat shape of ∞ coil

試作 ∞ コイルを、手動で移動させ、渦流探傷器 ET-5002 によって欠損に起因する信号を測定する。図 4 に示す ET-5002 は、センサが欠損上を移動するとき、ブリッジで信号を検出しリサージュ表示する。

励磁周波数を 2 kHz に設定し、リフトオフは 0.2mm から 3mm まで不規則な間隔で 5 点変更して測定した。また、ET-5002 の Gain、ハイパスフィルタ、ローパスフィルタをそれぞれ 60dB、off、10Hz に設定した。



図 4 過流探傷器(ET-5002)

Fig. 4. ET-5002 ECT signal processor made by Emic (Denshijiki Industry Co., Ltd).

〈3・2・2〉 実験結果

ET-5002 によって得られた検出信号波形を図 5 に示す。検出信号には 5 個のピークが存在し、裏面欠損付近をセンサが通過した場合の検出信号波形に対応する。5 個のピーク誘起電圧の大きさは 5 段階のリフトオフ位置に対応している。

図 5 から、リフトオフを 0.2mm から 3mm まで不規則な間隔で 5 点変更した場合、センサピーク誘起電圧はリフトオフに対して反比例する傾向が伺える。すなわち、リフトオフが大きくなればセンサピーク誘起電圧は減少する。

図 5 で、センサピーク誘起電圧は、リフトオフ 0.2、0.6、1、2、さらに 3mm に対してそれぞれ 2.95、2.52、2.02、1.59、0.93mV である。

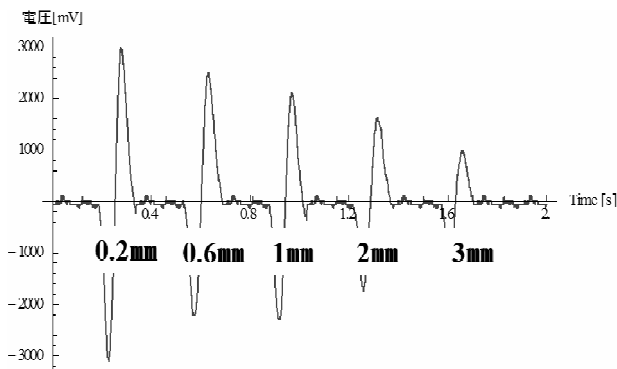


図 5 センサ誘起電圧とリフトオフの関係 (平面)

Fig.5. Induced voltage vs. lift-off (flat surface)

〈3・3〉 シミュレーションと実験値の比較

図 2 と図 5 を比較すると、概ねの減少傾向は一致しているが、センサピーク誘起電圧の値に差異がある。これらと比較するため、それぞれの絶対最大値を基準として正規化する。すなわち、図 2 と図 5 それぞれの絶対最大値でそれぞれの出力信号を割り算し、両者の最大値を 1 とし、両

者を比較する。図 6 が結果である。正規化された出力は、シミュレーションに拠ればリフトオフ 0.2、0.6、1、2、さらに 3mm に対してそれぞれ 1、0.86、0.75、0.61、0.43 である。他方、実験値に拠ればリフトオフ 0.2、0.6、1、2、さらに 3mm に対してそれぞれ 1、0.9、0.57、0.45、0.27 である。

図 6 から、リフトオフが大きくなると実験とシミュレーション値の相違が大きく、シミュレーションの方が大きな値をとる。これは、リフトオフが大きくなるほど実際の実験環境、すなわち、周辺に存在する実験機材が磁界分布に影響し、センサ感度を低下させることを示唆している。

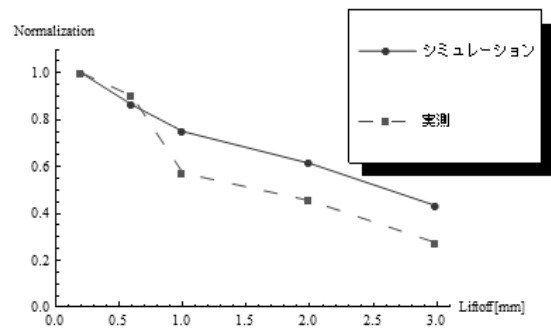


図 6 正規化したシミュレーションと実験値の比較

Fig.6 Comparison between the normalized simulation and experimental results.

4. 曲面状対象の裏面欠損探査実験

〈4・1〉 シミュレーションに依るリフトオフ特性

リフトオフを 0.2mm から 3mm まで変化した場合における曲面の検査対象のセンサ出力特性を吟味する。

曲面状被検査対象は厚さ 2mm の銅板からなり、裏面に幅 2mm、深さ 1mm の直線状欠損が存在する。図 7 は、三次元有限要素法のシミュレーションモデルを示し、励磁コイルと検出コイル、それぞれの諸定数は、表 1 と同様である。

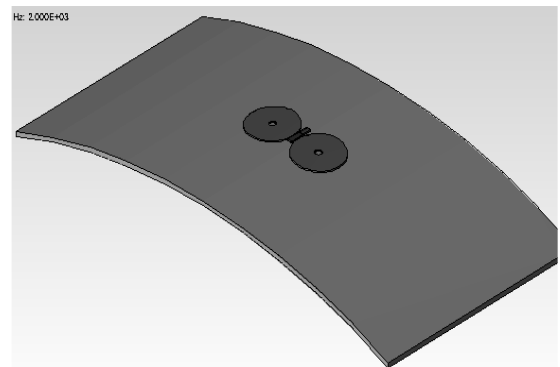


図 8 三次元有限要素シミュレーションの概略図

Fig. 8. Schematic diagram of the 3D FEM

図 8 はシミュレーションに拠る検出コイルのピーク誘起電圧とリフトオフの関係をしめす。

図8は、リフトオフを0.2mmから3mmまで不規則な間隔で5点変更した場合、センサピーク誘起電圧はリフトオフが2mmを境に減少し、全体としてセンサピーク誘起電圧はリフトオフ距離に反比例する傾向を示している。

図8で、センサピーク誘起電圧は、リフトオフ0.2、0.6、1、2、さらに3mmに対してそれぞれ3.56、2.98、2.63、1.61、1.33mVである。

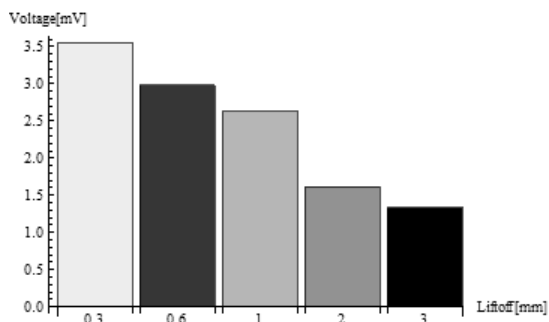


図8 シミュレーションによる
センサピーク電圧とリフトオフの関係
Fig. 8. Induced voltage vs. lift-off

〈4・2〉リフトオフ特性の実験

〈4・2・1〉実験方法

シミュレーション結果の妥当性を調べるため、表1の仕様で作成された諸定数の試作平面型のコイルのリフトオフ特性を実験する。

実験に採用した被検査対象である銅版を図9に示す。試作コイルは、図1と同一である。測定方法は平面裏面探査の場合と同様である。

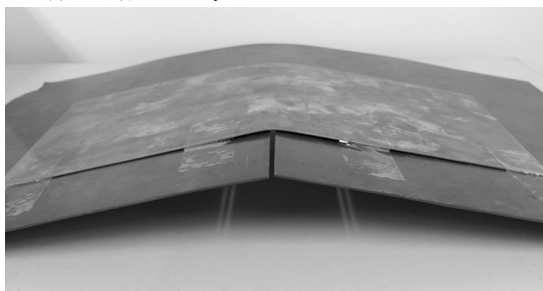


図9 被検査対象（曲面）
Fig.9. The target tested piece(curved surface)

ET-5002によって得られた検出信号波形を図9に示す。平面裏面探査と同様に検出信号には5個のピークが存在し、裏面欠損付近をセンサが通過した場合の検出信号に対応する。5個のピーク誘起電圧の大きさは5段階のリフトオフ位置に対応している。

図10は、リフトオフを0.2mmから3mmまで不規則な間隔で5点変更した場合、センサピーク誘起電圧はリフトオフに対して反比例する傾向を示す。すなわち、リフトオフが大きくなればセンサピーク誘起電圧は減少する。

図10で、センサピーク誘起電圧は、リフトオフ0.2、0.6、1、2、

さらに3mmに対してそれぞれ2.24、2.08、1.6、1.2、0.72mVである。

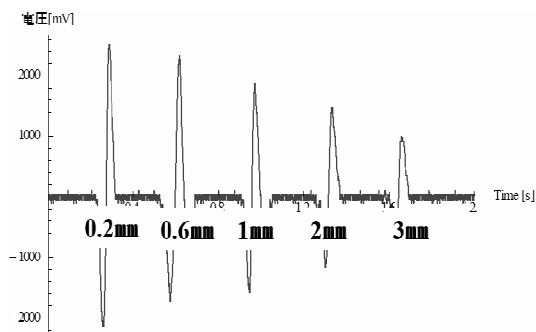


図10 センサ誘起電圧とリフトオフの関係(曲面)
Fig.10. Induced voltage vs. lift-off (curved surface)

〈4・3〉シミュレーションと実験値の比較

図8と図10を比較すると、リフトオフの増加と感度の減少傾向は両者で一致しているがわかる。

しかし、センサピーク誘起電圧の値に差異がある。これらを比較するため、平面状被検査対象の場合と同様に、シミュレーションと実験、それぞれの絶対最大値を基準値として正規化した。図11が結果である。正規化された出力は、シミュレーションに拠ればリフトオフ0.2、0.6、1、2、さらに3mmに対してそれぞれ1、0.86、0.75、0.61、0.43である。他方、実験値に拠ればそれぞれ1、0.9、0.57、0.45、0.27である。

図11から、リフトオフが大きくなっても実験とシミュレーション値の相違がほとんどなく、リフトオフの増加に対して感度が減少する反比例な傾向が伺える。

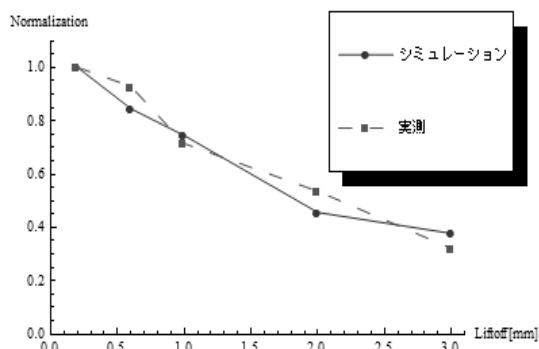


図11 シミュレーションと実測の正規化比較（曲面）
Fig.11 Comparison between the normalized simulation and experimental results.(curved surface)

図6と図11を比較すると、曲面探査の結果は平面探査に比較して、シミュレーションと実験値で差異が生じなかったのは、平面状励磁コイルが被検査対象を覆うように位置するため、感度が周辺に存在する機器の影響を受け難く。さらに、平面型に比較して曲面であるため、励磁磁束が通過する磁路が短くなり、結果として実験環境がシミュレー

ションと良く対応したためと考えられる。

5. 結論

本論文は低周波励磁平面型 ∞ コイルによる裏面欠損探傷に於けるリフトオフ特性について述べた。

低周波励磁 ∞ コイルの出力信号処理は ET-5002 で行った。シミュレーション結果と実験値を比較するため、シミュレーションと実験、それぞれの絶対最大値を基準として正規化した。

その結果、平面型 ∞ コイルの低周波励磁に拠る平面及び曲面の裏面探査に於けるリフトオフ特性は被検査対象が平面状か曲面状で異なり、シミュレーションは曲面状被検査対象に対して十分な精度有する。しかし、平面状被検査対象に対しては、リフトオフが大きくなるとシミュレーションは実験値を反映し難いことが判明した。

この原因は、曲面状被検査対象に対して、平面型 ∞ コイルの励磁コイルが被検査対象を覆うように変形可能であり、結果として、平面型 ∞ コイルの励磁コイルのフレキシビリティが実験に於ける周辺機器の影響を遮蔽する効果を発揮するためと考えられる。

て有利であることが判明した。

本論文の三次元有限要素法解析は JSOL 株式会社の「JMAG」で行なった。

文 献

- (1) 菊地原弘基、齋藤兆古、大内学、茂木秀夫、及川芳郎：「新 ∞ 型渦電流センサの開発」、第 21 回 MAGDA コンフェランス(仙台)、Os6-8、pp.181-185(2012)
- (2) Kouki, MARUYAMA, Iliana MARINOVA, Yoshifuru SAITO, Enhance the Sensibility of the Resonance type ECT Sensor, JAPMED'8, pp. 130-131.
- (3) Shunichi, HMANAKA, Iliana MARINOVA, Yoshifuru SAITO "Backside defect searching by means of the low frequency ∞ coil excitation", SIELA2014, pp.000-000 (2014)

以上のことから、平面型 ∞ コイルの低周波励磁に拠る裏面探査に於けるリフトオフ特性は、曲面状被検査対象に対し